



**US Army Corps  
of Engineers®**  
Engineer Research and  
Development Center



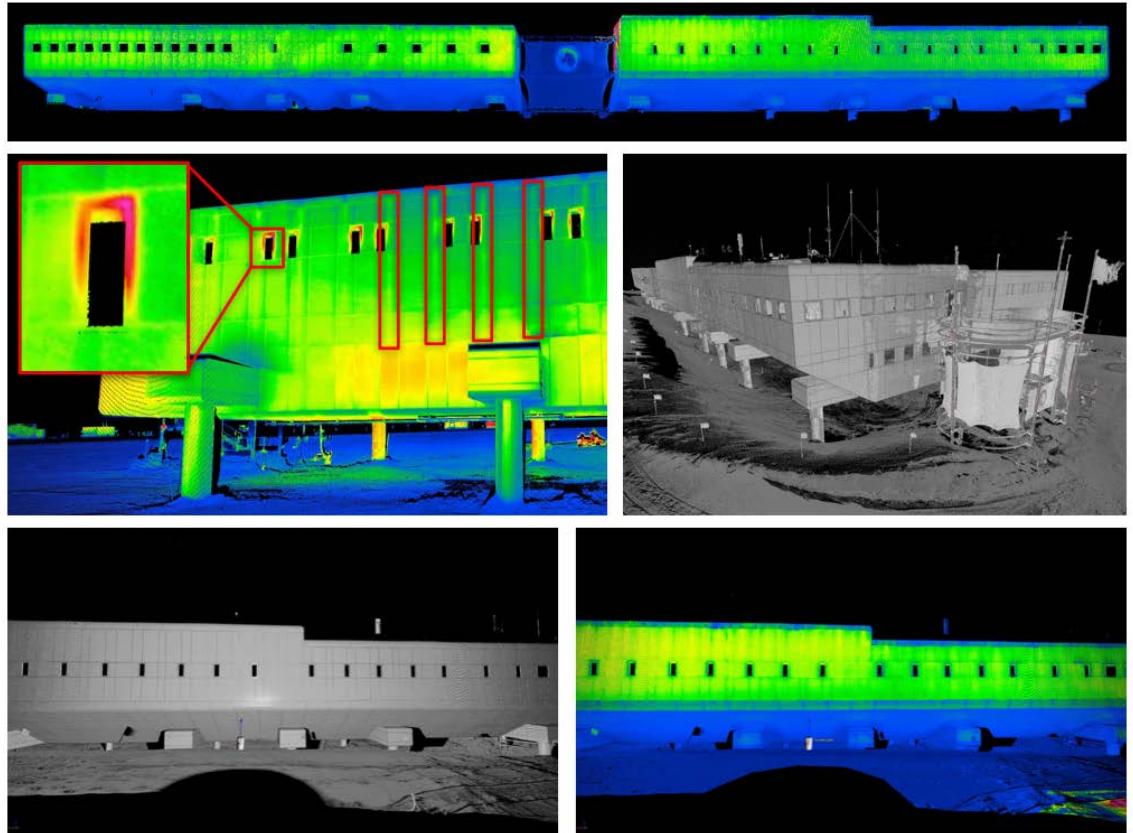
*Engineering for Polar Operations, Logistics, and Research (EPOLAR)*

# **Building Envelope and Infrastructure Assessment Using an Integrated Thermal Imaging and Lidar Scanning System**

Amundsen-Scott South Pole Station, Antarctica

Adam L. LeWinter, David C. Finnegan, Elias J. Deeb,  
and Peter J. Gadomski

June 2018



**The U.S. Army Engineer Research and Development Center (ERDC)** solves the nation's toughest engineering and environmental challenges. ERDC develops innovative solutions in civil and military engineering, geospatial sciences, water resources, and environmental sciences for the Army, the Department of Defense, civilian agencies, and our nation's public good. Find out more at [www.erdcenter.usace.army.mil](http://www.erdcenter.usace.army.mil).

To search for other technical reports published by ERDC, visit the ERDC online library at <http://acwc.sdp.sirsi.net/client/default>.

# **Building Envelope and Infrastructure Assessment Using an Integrated Thermal Imaging and Lidar Scanning System**

Amundsen-Scott South Pole Station, Antarctica

Adam L. LeWinter, David C. Finnegan, Elias J. Deeb, and Peter J. Gadomski

*U.S. Army Engineer Research and Development Center (ERDC)  
Cold Regions Research and Engineering Laboratory (CRREL)  
72 Lyme Road  
Hanover, NH 03755-1290*

Final Report

Approved for public release; distribution is unlimited.

Prepared for National Science Foundation, Office of Polar Programs  
2415 Eisenhower Avenue  
Alexandria, VA 22314

Under Engineering for Polar Operations, Logistics, and Research (EPOLAR)  
EP-ANT-16-07, “Building Envelope and Infrastructure Assessment Using an  
Integrated Thermal Imaging and Lidar Scanning System”

## Abstract

We conducted a combined lidar and Thermal Infrared (TIR) survey at the Amundsen-Scott South Pole Station, Antarctica, in January 2017 to assess the building thermal envelope and infrastructure of the Elevated Station. These coregistered data produce a three-dimensional (3-D) model with assigned temperature values for target surfaces, useful in spatially identifying thermal anomalies and areas for potential improvements. In addition, the accuracy of the resulting 3-D point cloud is useful for assessing building infrastructure by locating and quantifying areas of building settlement and structural anomalies. The lidar/TIR data collection was conducted in tandem with interior and exterior temperature and atmospheric measurement logging, handheld electro-optical imagery collection, and Global Navigation Satellite System real-time kinematic surveys to place the collected data in a global coordinate system. By analyzing the resulting data products, we conclude that while some thermal deficiencies exist, the building design and the material have maintained thermal-envelope integrity and display no significant thermal deficiencies. However, comparing building base elevations shows that significant and unequal settlement across the building has occurred. We suggest mitigating the thermal deficiencies through exterior repairs and that the building settlement be addressed in future leveling procedures to include lidar surveys.

**DISCLAIMER:** The contents of this report are not to be used for advertising, publication, or promotional purposes. Citation of trade names does not constitute an official endorsement or approval of the use of such commercial products. All product names and trademarks cited are the property of their respective owners. The findings of this report are not to be construed as an official Department of the Army position unless so designated by other authorized documents.

**DESTROY THIS REPORT WHEN NO LONGER NEEDED. DO NOT RETURN IT TO THE ORIGINATOR.**

# Contents

<b>Abstract .....</b>	<b>ii</b>
<b>Figures and Tables.....</b>	<b>v</b>
<b>Preface.....</b>	<b>ix</b>
<b>Acronyms and Abbreviations.....</b>	<b>x</b>
<b>Unit Conversion Factors .....</b>	<b>xi</b>
<b>1 Introduction.....</b>	<b>1</b>
1.1 Background.....	1
1.2 Objectives.....	2
1.3 Approach .....	3
<b>2 Lidar/TIR System Description .....</b>	<b>4</b>
2.1 Lidar scanner .....	4
2.2 Thermal infrared camera.....	5
2.3 Thermal jacket .....	6
<b>3 Data Acquisition.....</b>	<b>8</b>
3.1 External temperature measurements .....	9
3.2 Interior measurements.....	11
3.3 GNSS control survey.....	13
3.4 Handheld electro-optical imagery.....	14
3.5 Lidar/TIR system.....	15
<b>4 Data Processing.....</b>	<b>18</b>
4.1 Lidar scans registration and georeferencing .....	18
4.2 Thermal infrared radiometric value registration .....	20
4.3 Data products .....	20
<b>5 Results and Discussion.....</b>	<b>22</b>
5.1 Solar-exposure limitations.....	22
5.2 Exterior surface thermal analysis .....	23
5.3 Elevated Station structural assessment.....	36
<b>6 Conclusion and Recommendations .....</b>	<b>41</b>
<b>References .....</b>	<b>43</b>
<b>Appendix A : Lidar/TIR System Thermal Jacket Design.....</b>	<b>44</b>
<b>Appendix B : 2017 Lidar/TIR Survey Map.....</b>	<b>47</b>
<b>Appendix C : CRREL Lidar/TIR System Data Acquisition Procedure .....</b>	<b>49</b>

---

<b>Appendix D : 2017 Lidar/TIR Survey Notes .....</b>	<b>52</b>
<b>Appendix E : South Pole Elevated Station Lidar/TIR Survey: Lidar Processing Notes .....</b>	<b>54</b>
<b>Appendix F : 2017-01-SouthPole Processing Report .....</b>	<b>57</b>
<b>Appendix G : Elevated Station Column Height Elevation Plots.....</b>	<b>59</b>
<b>Report Documentation Page</b>	

# Figures and Tables

## Figures

1	Riegl VZ-1000 TLS lidar scanner (front and side views) used in the lidar/TIR system. The sensor is portable and light enough for one person to carry and setup in the field .....	4
2	<i>Left:</i> Field-of-view of the lidar sensor ( <i>blue shaded area</i> ) compared with the FOV of the TIR ( <i>red shaded area</i> ). While the lidar sensor has a wider FOV, the typical setup of the system places the focus object (building) within the narrower TIR FOV, providing full coverage from both sensors. <i>Right:</i> Lidar/TIR system in use .....	5
3	Panoramic thermal image, colored by temperature ( $-50^{\circ}\text{C}$ to $-15^{\circ}\text{C}$ ), of the South Pole Elevated Station taken from Scan Position 3 .....	6
4	<i>Left:</i> CAD (computer-aided design) model of the thermal jacket design concept for the lidar/TIR system. Gray panels represent permanent surfaces when installed while <i>blue</i> panels are removable for system operation. <i>Right:</i> Final thermal jacket system deployed at South Pole Station.....	7
5	Survey map indicating the location of scan positions, GNSS base station and reflectors, electro-optical image acquisition positions, and external air temperature sensor placement.....	8
6	Air temperature measurements from eight sensors temporarily installed around the exterior of the South Pole Elevated Station during the lidar/TIR survey .....	10
7	Plot of air temperature measurements for 17–19 January 2017 from the South Pole Observatory meteorological station, taken from 2 m above the snow surface .....	10
8	Plot of air temperature measurements for 17–19 January 2017 from all HOBO air temperature sensors and the South Pole Observatory meteorological station .....	11
9	Example of interior air temperature measurements logged in Pod A2 of the Elevated Station (second, first, and subfloors). The <i>red stars</i> indicate the locations of temperature measurements plotted to the right of the floorplans .....	12
10	A 10 cm cylinder reflector setup during the South Pole lidar/TIR survey. The reflectors, with 10 cm height/diameter dimensions, provide reference coordinates used to tie the 3-D model to a global coordinate system.....	13
11	A 10 cm reflector cylinder with Trimble R8 antenna setup, highlighting the need to apply a height offset from the antenna measurement point to the cylinder centroid .....	14
12	Electro-optical image ( <i>left</i> ) captured from scan position 20 compared to the reflectance-colored 3-D model ( <i>right</i> ), highlighting the utility of capturing true-color images in conjunction with the lidar/TIR data acquisition.....	14
13	Author David Finnegan operating CRREL's lidar/TIR system at the South Pole Station. The thermal jacket was designed specifically for this survey, maintaining the minimum operating temperatures for both sensors. A generator, housed in the enclosure located on the snowmobile sled, provides power to both the system and the thermal jacket .....	15
14	Example data from scan position 3. <i>Top:</i> 2-D view of lidar data, colored by surface reflectance. More reflective surfaces backscatter stronger laser returns. <i>Bottom:</i> Set of TIR images collected, colored by a $-45^{\circ}\text{C}$ to $-5^{\circ}\text{C}$ color scale .....	16
15	Visualization of the coarse registration process in which an unregistered scan is roughly aligned to a registered, georeferenced baseline scan. Scan position 22	

	( <i>right</i> ) was tied to the UPS South coordinate system using reflectors and the GNSS RTK survey. Scan position 21 ( <i>left</i> ) was captured from a similar position as 22 and therefore has significant overlap.....	19
16	Lidar data of the Elevated Station was collected from 22 different scan positions. Each resulting point cloud covered a portion of the Station. The <i>top</i> image shows eight of these point clouds, colored by scan position. After registration/georeferencing, the individual scans combine to create a complete 3-D model of the Station ( <i>bottom</i> ).....	19
17	A 3-D model captured from scan position 4 colored by surface reflectance ( <i>left</i> ) and temperature ( <i>right</i> ). Mapping the TIR imagery onto the 3-D model visually represents thermal variations .....	20
18	A 3-D thermal model colored by temperature ( $-45^{\circ}\text{C}$ to $-5^{\circ}\text{C}$ ) taken during a period with direct sun exposure on a portion of the Elevated Station exterior.....	22
19	A thermal image of wing B1 taken from scan position 17. Because of direct solar exposure on the end wall, the thermal values are elevated, reducing the level of detail visible across a wider temperature scale of $-45^{\circ}\text{C}$ to $-5^{\circ}\text{C}$ ( <i>left</i> ). By altering the temperature scale of the thermal image ( $-15^{\circ}\text{C}$ to $20^{\circ}\text{C}$ ) to optimize detail in the solar-exposed sections, relative thermal differences are apparent ( <i>right</i> ).....	23
20	Comparison of Palmer Station and South Pole Station lidar/TIR results. <i>Left</i> : Palmer Station Biolab, $5^{\circ}\text{C}$ to $-15^{\circ}\text{C}$ scale. <i>Middle</i> : Palmer Station GWR (garage, warehouse, and recreation) building, $5^{\circ}\text{C}$ to $-15^{\circ}\text{C}$ scale. <i>Right</i> : South Pole Station Wing B3 North, $5^{\circ}\text{C}$ to $-45^{\circ}\text{C}$ scale.....	23
21	A 3-D thermal model of Wings A2/A3. <i>Top left</i> : Focus section highlighted in <i>red</i> on the Elevated Station map. <i>Bottom</i> : North side of Wings A2 and A3, $-40^{\circ}\text{C}$ to $-15^{\circ}\text{C}$ scale. <i>Top right</i> : Underside view of a piece of detached trim identified initially by its lower temperature.....	24
22	A 3-D thermal model of Wing A3 West. <i>Top left</i> : Focus section highlighted in <i>red</i> on the Elevated Station map. <i>Bottom</i> : Wing A3 West at a $-40^{\circ}\text{C}$ to $-15^{\circ}\text{C}$ scale.....	24
23	A 3-D thermal model of Wing B2 East. <i>Top left</i> : Focus section highlighted in <i>red</i> on the Elevated Station map. <i>Bottom</i> : Wing B2 East at a $-40^{\circ}\text{C}$ to $-5^{\circ}\text{C}$ scale. ....	25
24	A 3-D thermal model of Wing B2 North. <i>Top left</i> : Focus section highlighted in <i>red</i> on the Elevated Station map. <i>Bottom</i> : Wing B2 North at a $-40^{\circ}\text{C}$ to $-15^{\circ}\text{C}$ scale.....	25
25	A 3-D thermal model of Wing B3 North. <i>Top left</i> : Focus section highlighted in <i>red</i> on the Elevated Station map. <i>Bottom</i> : Wing B3 North at a $-40^{\circ}\text{C}$ to $-20^{\circ}\text{C}$ scale. Trim detachment was identified on the fourth window from the right ( <i>red square</i> ) and on two vertical trim pieces ( <i>top right</i> ).....	26
26	Wing B3 North SIP trim detachment. Temperature variation at SIP trim, allowing identification of trim fit issues and/or damage. The electro-optical image confirms the trim piece in question is dislodged from the SIPs.....	26
27	A 3-D thermal model of Wing B3 West and portion of Observation Deck Destination Alpha. <i>Top left</i> : Focus section highlighted in <i>red</i> on the Elevated Station map. <i>Bottom</i> : Wing B3 West at a $-40^{\circ}\text{C}$ to $-20^{\circ}\text{C}$ scale .....	27
28	A 3-D thermal model of Wing B4 West. <i>Top left</i> : Focus section highlighted in <i>red</i> on the Elevated Station map. <i>Bottom</i> : Wing B4 West at a $-35^{\circ}\text{C}$ to $-5^{\circ}\text{C}$ scale. The <i>red box</i> indicates windows with high thermal gradients above and along the sides of the frames. <i>Top right</i> : Detail view of the windows in questions .....	27
29	A 3-D thermal model of Wing B4 South. <i>Top left</i> : Focus section highlighted in <i>red</i> on the Elevated Station map. <i>Bottom</i> : Wing B4 South at a $-15^{\circ}\text{C}$ to $15^{\circ}\text{C}$ scale.....	28

30	A 3-D thermal model of Wing B4 East. <i>Top left:</i> Focus section highlighted in <i>red</i> on the Elevated Station map. <i>Bottom:</i> Wing B4 South at a $-15^{\circ}\text{C}$ to $-5^{\circ}\text{C}$ scale. <i>Top:</i> Wing B4 South at a $-40^{\circ}\text{C}$ to $-10^{\circ}\text{C}$ scale.....	28
31	Wing B4 East. The four <i>red vertical rectangles</i> encompass areas of thermal bridging from the building frame structure, with measurements of up to $4^{\circ}\text{C}$ difference across the bridging sections. The enlarged window ( <i>inset image</i> ) identifies an area of heat loss of up to $20^{\circ}\text{C}$ difference ( $-29^{\circ}\text{C}$ to $-9^{\circ}\text{C}$ ) .....	29
32	A 3-D thermal model of Wing B2/B3 South. <i>Top left:</i> Focus section highlighted in <i>red</i> on the Elevated Station map. <i>Bottom:</i> Wing B2/B3 South at a $-45^{\circ}\text{C}$ to $20^{\circ}\text{C}$ scale .....	29
33	A 3-D thermal model of Wing B1 West. <i>Top left:</i> Focus section highlighted in <i>red</i> on the Elevated Station map. <i>Bottom:</i> Wing B1 West at a $-40^{\circ}\text{C}$ to $-10^{\circ}\text{C}$ scale.....	30
34	A 3-D thermal model of Wing B1 South. <i>Top left:</i> Focus section highlighted in <i>red</i> on the Elevated Station map. <i>Bottom:</i> Left and right views of Wing B4 South at a $-15^{\circ}\text{C}$ to $15^{\circ}\text{C}$ scale.....	30
35	A 3-D thermal model of Wing B1 East. <i>Top left:</i> Focus section highlighted in <i>red</i> on the Elevated Station map. <i>Bottom:</i> Wing B1 East at a $-40^{\circ}\text{C}$ to $-15^{\circ}\text{C}$ scale. <i>Top right:</i> Detail of a generator exhaust vent at a $-40^{\circ}\text{C}$ to $20^{\circ}\text{C}$ scale.....	31
36	A 3-D thermal model of Pod A/B Connector South. <i>Top left:</i> Focus section highlighted in <i>red</i> on the Elevated Station map. <i>Bottom:</i> Pod A/B Connector South at a $-40^{\circ}\text{C}$ to $15^{\circ}\text{C}$ scale .....	31
37	A 3-D thermal model of Wing A4 West. <i>Top left:</i> Focus section highlighted in <i>red</i> on the Elevated Station map. <i>Bottom:</i> Wing A4 West at a $-40^{\circ}\text{C}$ to $-10^{\circ}\text{C}$ scale .....	32
38	A 3-D thermal model of Wing A4 South. <i>Top left:</i> Focus section highlighted in <i>red</i> on the Elevated Station map. <i>Bottom:</i> Left and right views of Wing A4 South at a $-15^{\circ}\text{C}$ to $15^{\circ}\text{C}$ scale .....	32
39	A 3-D thermal model of Wing A4 East. <i>Top left:</i> Focus section highlighted in <i>red</i> on the Elevated Station map. <i>Bottom:</i> Wing B1 East at a $-40^{\circ}\text{C}$ to $-10^{\circ}\text{C}$ scale.....	33
40	A 3-D thermal model of Wing A2/A3 South and Destination Zulu. <i>Top left:</i> Focus section highlighted in <i>red</i> on the Elevated Station map. <i>Bottom:</i> Wing A2/A3 South at a $-40^{\circ}\text{C}$ to $-15^{\circ}\text{C}$ scale.....	33
41	A 3-D thermal model of Wing A1 West. <i>Top left:</i> Focus section highlighted in <i>red</i> on the Elevated Station map. <i>Bottom:</i> Wing A1 West at a $-40^{\circ}\text{C}$ to $-10^{\circ}\text{C}$ scale. ....	34
42	A 3-D thermal model of Wing A1 South. <i>Top left:</i> Focus section highlighted in <i>red</i> on the Elevated Station map. <i>Bottom:</i> Left and right views of Wing A1 South at a $-15^{\circ}\text{C}$ to $15^{\circ}\text{C}$ scale.....	34
43	A 3-D thermal model of Wing A1 East. <i>Top left:</i> Focus section highlighted in <i>red</i> on the Elevated Station map. <i>Bottom:</i> Wing B1 East at a $-40^{\circ}\text{C}$ to $-10^{\circ}\text{C}$ scale.....	35
44	A 3-D thermal model of the Vertical Tower South. <i>Top left:</i> Focus section highlighted in <i>red</i> on the Elevated Station map. <i>Bottom:</i> Vertical Tower South at a $-40^{\circ}\text{C}$ to $20^{\circ}\text{C}$ scale .....	35
45	A 3-D thermal model of the Vertical Tower North and Wing A2 East. <i>Top left:</i> Focus section highlighted in <i>red</i> on the Elevated Station map. <i>Bottom:</i> Vertical Tower North and Wing A2 East at a $-40^{\circ}\text{C}$ to $10^{\circ}\text{C}$ scale .....	36
46	Measured height differences between adjacent support columns of the South Pole Elevated Station from the 5 February 2017 traditional survey .....	37
47	A point cloud side view of an isolated column from the Elevated Station, colored by surface reflectance .....	38

48 Measured height differences between adjacent support columns of the South Pole Elevated Station from the 17–18 January 2017 lidar survey.....38

49 *Top*: Bottom surface of the Elevated Station isolated and colored by height (*blue* to *red* = 9,316.10 ft to 9,316.83 ft), clearly showing areas of settlement and building slope. *Bottom left*: Sagging of SIP is visible as gridded low points. *Bottom right*: Apparent frame structure is visible as orthogonal height points (*red grid*) .....40

G-1 February 5, 2017 Elevated Station column height difference map .....59

G-2 January 17–18, 2017 Elevated Station column height difference map .....60

**Tables**

1 Comparison between lidar-derived column angle bar measurements (17–18 January 2017) and traditional column survey measurements (5 February 2017). Values (inches) are the 5 February results subtracted from the 17–18 January results .....39

## Preface

This study was conducted for the National Science Foundation, Office of Polar Programs (NSF-OPP), under Engineering for Polar Operations, Logistics, and Research (EPOLAR) EP-ANT-16-07, “Building Envelope and Infrastructure Assessment Using an Integrated Thermal Imaging and Lidar Scanning System.” The technical monitor was Ms. Margaret Knuth, Program Manager, NSF-OPP, U.S. Antarctic Program.

The work was performed by the Lidar and Wetlands Group (CEERD-RRC) of the Remote Sensing and Geographical Information Systems Center of Expertise (CEERD-RZR), U.S. Army Engineer Research and Development Center, Cold Regions Research and Engineering Laboratory (ERDC-CRREL). At the time of publication, Dr. Elias Deeb was lead for the Lidar and Wetlands Group; Mr. David Finnegan was Chief, CEERD-RS; and Ms. Janet Hardy was the program manager for EPOLAR. The Deputy Director of ERDC-CRREL was Mr. David B. Ringelberg, and the Director was Dr. Joseph L. Corriveau.

COL Bryan S. Green was Commander of ERDC, and Dr. David W. Pittman was the Director.

## Acronyms and Abbreviations

AC	Alternating Current
AIL	Antarctic Infrastructure and Logistics
CAD	Computer-Aided Design
CRREL	U.S. Army Cold Regions Research and Engineering Laboratory
ERDC	Engineer Research and Development Center
FOV	Field of View
GNSS	Global Navigation Satellite System
GRiD	Geospatial Repository and Data Management System
GWR	Garage, Warehouse, and Recreation
MSA	Multi-Station Adjustment
NSF	National Science Foundation
OPP	Office of Polar Programs
RGB	Red-Green-Blue
RTK	Real-Time Kinematic
SIP	Structural Insulated Panel
SPO	South Pole Observatories
3-D	Three Dimensional
TIR	Thermal Infrared
TLS	Terrestrial Laser Scanner
UPS	Universal Polar Stereographic
USAP	U.S. Antarctic Program
VAC	Voltage Alternating Current

## Unit Conversion Factors

Multiply	By	To Obtain
bars	100	kilopascals
degrees (angle)	0.01745329	radians
degrees Fahrenheit	$(F-32)/1.8$	degrees Celsius
feet	0.3048	meters
inches	0.0254	meters
microinches	0.0254	micrometers
microns	1.0 E-06	meters
miles (U.S. statute)	1,609.347	meters
miles per hour	0.44704	meters per second
pounds (mass)	0.45359237	kilograms
yards	0.9144	meters



# 1 Introduction

## 1.1 Background

Located at the Amundsen-Scott South Pole Station, the Elevated Station building is in one of the most cold, remote and austere environments in Antarctica. This increases the challenges faced when maintaining building temperatures at a comfortable working level and the difficulty, and therefore cost, of supplying the station with heating fuel. Energy efficiency of building infrastructure plays a crucial role in operating remote stations for the U.S. Antarctic Program (USAP). The National Science Foundation, Office of Polar Programs, Antarctic Infrastructure and Logistics (NSF-OPP-AIL), has identified this as a key priority.

As part of the major infrastructure replacement and upgrades at South Pole Antarctic Infrastructure Modernization for Science, it is prudent to assess existing infrastructure in an effort to evaluate the current condition, potential maintenance required, and architectural design performance in the harsh Antarctic environment. In FY15, NSF-OPP-AIL funded an effort to characterize building envelopes and assess building energy efficiency at Palmer Station (Deeb and LeWinter 2018). This effort used a thermal infrared (TIR) and lidar scanning system designed and integrated by the U.S. Army Cold Regions Research and Engineering Laboratory (CRREL) and advanced processing techniques to fuse these disparate datasets. The system combines both spatial and thermal measurements of target surfaces as a comprehensive tool for assessing building envelopes and a means of separating geometric and radiometric influences from one another.

TIR, or thermography, is a passive, nondestructive and stand-off method to identify thermal variations across building surfaces that contribute to heat loss and building inefficiencies. With a highly sensitive (0.05 K at 30°C) detector, small thermal anomalies can be quantified. Lidar is a fast and accurate technology capable of obtaining three-dimensional (3-D) measurements at high spatial and temporal resolutions with millimeter-scale accuracy and ranges exceeding 6 km from a ground-based sensor. In addition, the lidar also measures surface reflectance values at each meas-

ured surface point, corresponding to wavelength characteristics and surface reflectance properties (wood, aluminum, concrete, etc.). Because the surface reflectance of the transmitted laser pulse varies with different building materials, a comparison between the reflectance and thermal values helps to identify building materials that are more or less energy efficient. In addition, the resulting 3-D point cloud may be used to make precise measurements, to identify areas of change when referenced to previously collected data, and to compare with architectural drawings for assessing construction quality. Furthermore, when collected with high-accuracy Global Navigation Satellite System (GNSS) position data, it is possible to tie the point cloud to a global coordinate system.

TIR and lidar surveys are commonplace in the fields of building envelope assessments and spatial measurements, respectively. Phetteplace (2007) presented findings from an infrared surveys conducted between 2005 and 2007 of the Elevated Station. However, if collected independently, it is both labor intensive and difficult to merge these datasets to produce a 3-D thermal model. With CRREL's integrated lidar/TIR system, these two disparate datasets are collected coincidentally. With known spatial relations and error between sensors, along with laser and camera calibrations, it is possible to accurately combine these measurements. By combining the data products derived from TIR, lidar, and GNSS, a 3-D thermal model is produced that includes the thermal signature, a range-independent surface reflectance value, and an absolute location for each individual measurement in space.

## 1.2 Objectives

For this effort, we aimed to deploy the lidar/TIR system during the austral summer to conduct surveys of the South Pole Elevated Station building infrastructure. From these data, CRREL can provide comprehensive 3-D models with thermal signatures assigned to each individual lidar point measurement. These data may then be used to assess the building envelope by identifying any thermal anomalies, which indicate a deficiency in the insulation or building material and design, and to identify any infrastructure concerns due to building settlement and ice-sheet movement.

A second objective of this effort was to develop a system capable of operating in extreme cold. The minimum operating temperatures for the lidar scanner and TIR camera are  $-10^{\circ}\text{C}$  and  $-15^{\circ}\text{C}$ , respectively. Daily mean temperatures in January for South Pole Station range from approximately

25°C to −35°C (based on a 50-year climatology study [Lazzara et al. 2012]). Therefore, it is necessary to actively heat the lidar/TIR system during January collection operations. To accomplish this, we developed a thermal jacket to actively heat the system, keeping both sensors above their minimum operating temperatures. Local testing was performed prior to deployment, using both cold rooms and sufficiently cold exterior temperatures, to ensure that the thermal jacket provided sufficient heating.

### 1.3 Approach

To realize the objectives of this effort, we carried out the following tasks:

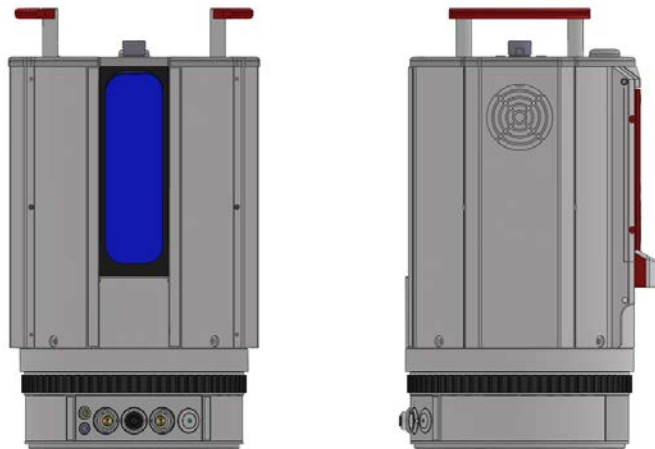
- Designed and tested a thermal jacket to actively heat the lidar/TIR system, maintaining temperatures above the manufacturer recommended minimum operating temperatures specified for each sensor—The thermal jacket did not obstruct the field-of-view for either sensor, preserving full system acquisition capabilities.
- Deployed the lidar/TIR system to South Pole Station in January 2017 to collect thermal and spatial measurements of the exterior of the Elevated Station, including initial data processing to ensure sufficient coverage of the building exterior—These data were tied to a global coordinate system (universal polar stereographic coordinate system—UPS South) utilizing GNSS real-time kinematic (RTK) equipment.
- Collected interior and exterior environmental conditions by using existing measurement infrastructure (permanent weather stations and interior temperature sensors) alongside temporarily deployed temperature and relative humidity sensors
- Used a handheld electro-optical camera (Nikon D800) to collect standard imagery for both reference and documentation of identified areas of thermal deficiencies
- Processed all collected data, combining the lidar, TIR, and GNSS measurements to produce a 3-D thermal model (LAZ file format) of the Elevated Station exterior
- Analyzed the resulting data to identify building envelope anomalies, deficiencies, and infrastructure concerns—From this data, we suggest courses of action to mitigate any identified issues and to confirm the effectiveness of current building material and design techniques.

## 2 Lidar/TIR System Description

### 2.1 Lidar scanner

We chose a Riegl VZ-1000 terrestrial laser scanner (TLS) as the lidar sensor (Figure 1), which had performed well when deployed in 2015 at Palmer Station. The VZ-1000 also provides the mounting platform, rotating stage, and power supply for the TIR sensor. The VZ-1000 is a full-waveform, time-of-flight sensor capable of capturing multiple range measurements per individual laser pulse. This better represents measured surfaces compared to discrete or single-return lidar sensors by capturing a higher point density (typically measured by points per square meter) and allowing for measurements through partially obstructing objects (fencing, windows, and blowing snow). The sensor uses a 1550 nm wavelength pulsed laser (Class 1 laser, eye safe) to measure range and surface reflectance of target objects. With a  $360^\circ \times 100^\circ$  (horizontal and vertical, respectively) field of view (FOV) and a maximum pulse rate of 300 kHz, the scanner captures a full FOV in as little as 8 seconds with a maximum measurement range of 1400 m and an accuracy and precision of 8 mm and 5 mm, respectively.

Figure 1. Riegl VZ-1000 TLS lidar scanner (front and side views) used in the lidar/TIR system. The sensor is portable and light enough for one person to carry and setup in the field.



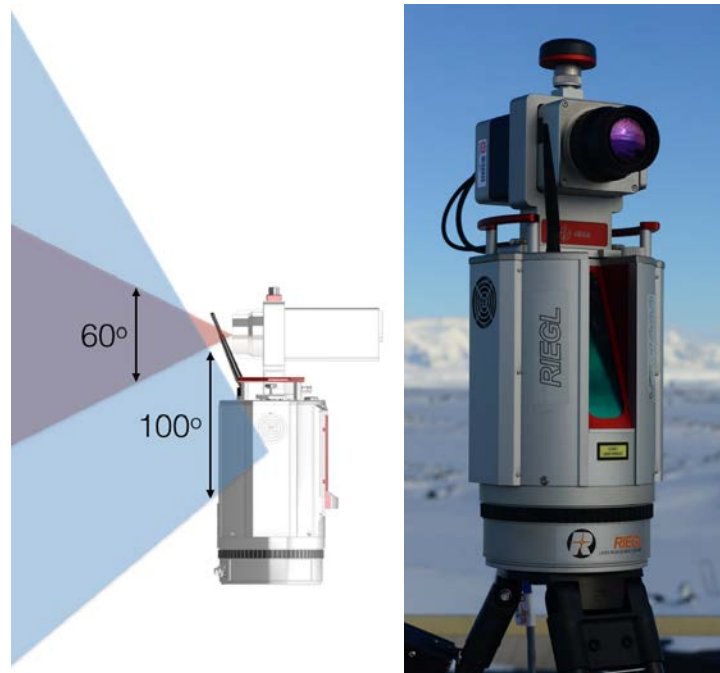
The acquisition parameters, including laser pulse rate and angular step width (vertical/horizontal angle between consecutive laser pulses) for the scanner are configurable based on the desired measurement range, time of scan acquisition, target-object albedo, and resulting point density. At the highest pulse rate (300 kHz) and smallest angular increment ( $0.0024^\circ$ ),

the scanner is capable of capturing tens of thousands of point measurements per square meter, resulting in subcentimeter point spacing.

## 2.2 Thermal infrared camera

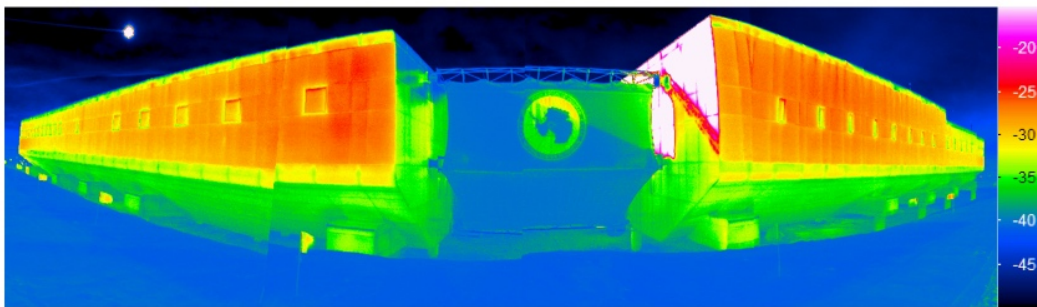
Hard mounted on the top of the lidar sensor is an InfraTec VarioCAM HD 880 thermal infrared camera. Using an uncooled microbolometer,  $1024 \times 768$  pixel focal-plane array with a  $7.5\text{--}14\ \mu\text{m}$  spectral range, the camera has a measurement range of  $-40^{\circ}\text{C}$  to  $1200^{\circ}\text{C}$ , a measurement accuracy of  $\pm 1.5\%$  of reading when surface temperatures are below  $0^{\circ}\text{C}$ , and a thermal resolution better than  $0.05\ \text{K}$  at  $30^{\circ}\text{C}$  (Figure 2). To best match the lidar vertical FOV ( $100^{\circ}$ ), a wide-angle  $15\ \text{mm}$  lens ( $60^{\circ} \times 47^{\circ}$  FOV) was used. By mounting the camera in a portrait orientation (camera rotated  $90^{\circ}$ ) onto the lidar sensor, this produces a  $10^{\circ}$  and  $30^{\circ}$  shadow below and above level, respectively, compared to the lidar data (Figure 2). To mitigate this data shadow, the system setup positions were selected to keep the building within the TIR FOV with multiple setup positions used to fully capture the target surfaces.

Figure 2. *Left:* Field-of-view of the lidar sensor (*blue shaded area*) compared with the FOV of the TIR (*red shaded area*). While the lidar sensor has a wider FOV, the typical setup of the system places the focus object (building) within the narrower TIR FOV, providing full coverage from both sensors. *Right:* Lidar/TIR system in use.



For the best control of TIR image acquisition, the camera is operated independently from the lidar scanner, relying on the scanner only for power and system rotation, allowing for full panoramic image acquisition. The resulting images are output in a proprietary .irb file format, which is imported into InfraTec's IRBIS 3 software package, built to support image analysis and exploitation of InfraTec TIR imagery (Figure 3). These images preserve per pixel calibrated radiometric values (temperature), which are converted to absolute temperature values. These images are then exported for further use.

Figure 3. Panoramic thermal image, colored by temperature ( $-50^{\circ}\text{C}$  to  $-15^{\circ}\text{C}$ ), of the South Pole Elevated Station taken from Scan Position 3. The image is composed from five individual images collected by the TIR camera. The image captures consistent temperature values on similarly oriented building surfaces. The breezeway cover (with USAP logo) and right side of the building show the influence of direct solar exposure on radiometric readings through high temperature measurements, shown as white surfaces.

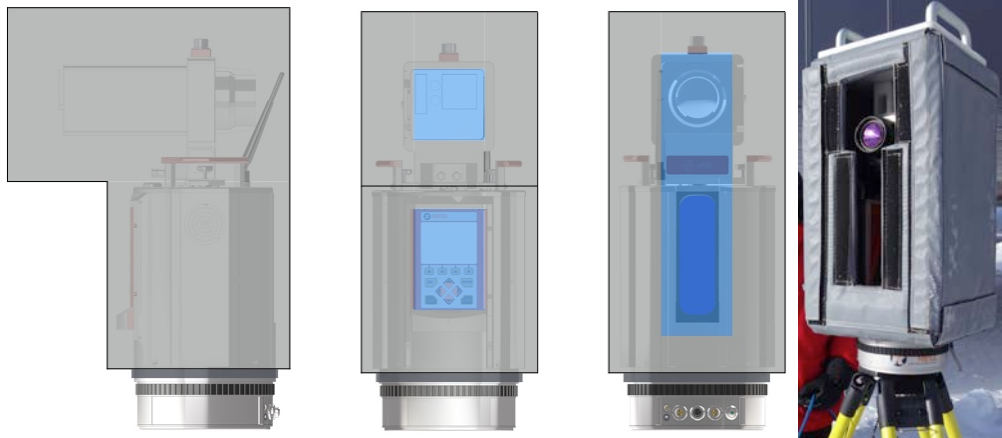


### 2.3 Thermal jacket

Because of expected temperatures below the minimum operating temperatures of both the lidar and TIR sensors, it was necessary to actively heat the system to prevent failures. Therefore, we designed a thermal jacket capable of actively heating the system (See Appendix A for design requirements drawing). Figure 4 shows the design concept and final thermal jacket. The thermal jacket consists of two 60 W 110VAC (voltage alternating current) heating elements requiring 40W controlled by an internal thermostat with on/off temperature settings of  $4^{\circ}\text{C}/15^{\circ}\text{C}$ . Power is supplied by a portable AC (alternating current) power generator. The jacket exterior and interior surfaces are made of a Teflon/fiberglass composite cloth with a Pyrogel XTE insulation core. The jacket is composed of ten panels connected by Velcro tabs, allowing the jacket to be flat-packed for transportation. For structural rigidity, transport, and coupling to the lidar/TIR system, we fabricated nylon plates designed to connect the jacket to the top of the system via an external GPS antenna connection. Cover panels (three) may be attached to close the jacket between data acquisition

to retain heat. When installed, the thermal jacket rotates freely with the lidar/TIR system and does not obstruct the FOV of either sensor.

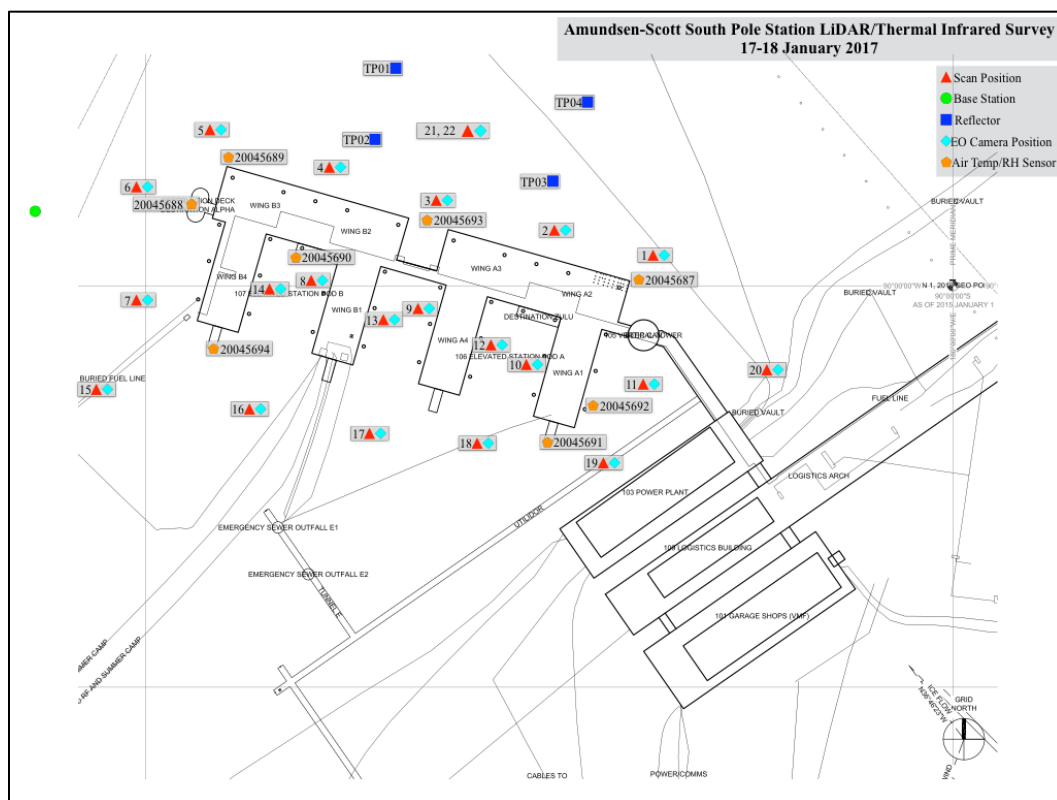
Figure 4. *Left*: CAD (computer-aided design) model of the thermal jacket design concept for the lidar/TIR system. *Gray* panels represent permanent surfaces when installed while *blue* panels are removable for system operation. *Right*: Final thermal jacket system deployed at South Pole Station. The front panels are removed for data acquisition, and the nylon plate on the top of the jacket provided structural rigidity and handles for transport.



### 3 Data Acquisition

We collected survey data on 17–19 January 2017 (Figure 5). While we made every effort to collect these data in stable, consistent environmental conditions (wind, solar exposure, cloud cover, lack of precipitation, etc.), the challenges of rapidly changing atmospheric conditions and the reality of a full 24 hours of daylight resulted in variations of thermal conditions throughout the acquisition. The effects of these variations, especially that of direct solar exposure during the TIR measurements, are discussed in the “Results and Discussion” portion of this report.

Figure 5. Survey map indicating the location of scan positions (*red triangles*), GNSS base station and reflectors (*green circle* and *blue squares*, respectively), electro-optical image acquisition positions (*aqua diamonds*), and external air temperature sensor placement (*orange pentagons*).



Along with the lidar/TIR data acquisition and GNSS measurements, we performed additional on-site measurements to support processing and analysis of the 3-D thermal building envelope. In particular, interior and exterior temperature measurements aid in the analysis of the building performance with respect to temperature gradients from inside the Elevated Station to the external surfaces. In addition to placing temporary sensors

outside of the building, we leveraged the extensive environmental monitoring built into the Elevated Station and received temperature logs from multiple locations from station management. Further, in an effort to provide visual context to potential areas of interest within the 3-D model, we captured images from each scan position and of any identified thermal anomalies by using a handheld digital SLR camera. Figure 5 shows the distribution of measurements with respect to the Elevated Station; Appendix B provides this in large format.

### 3.1 External temperature measurements

A set of eight HOBO Pro v2 sensors were temporarily distributed outside to log exterior air temperatures from different aspects of the building during the survey. The sensors, which are housed in a weatherproof enclosure and have internal logging capability, a temperature measurement range of  $-40^{\circ}\text{C}$  to  $70^{\circ}\text{C}$ , an accuracy of  $\pm 0.21^{\circ}\text{C}$  over  $0^{\circ}\text{C}$ – $50^{\circ}\text{C}$ , and a resolution of  $\pm 0.02^{\circ}\text{C}$ , were sampled at 1Hz. Refer to Appendix B and Figure 5 for placement locations.

Figure 6 shows a plot of all external air temperature measurements during the survey period. Variations in temperature measurements are due to different conditions at each location, including aspect, solar exposure, wind, and proximity to warmer objects (e.g., building surfaces, vehicles, and infrastructure). These measurements are referenced when assessing the 3-D thermal model, providing in situ data for comparing and validating TIR measurements and thermal-deficiency findings.

In addition to our air temperature sensors, external meteorological measurements are collected by the South Pole Observatory (SPO), part of the National Oceanic and Atmospheric Administration, Earth System Research Laboratory, and Global Monitoring Division Baseline Observatories (Vasel 2018). Meteorological measurements began in 1975 (wind speed and direction) with the addition of air temperature, relative humidity, and barometric pressure in 1975. Figure 7 shows air temperatures from the SPO station for 17–19 January 2017. During this period, there were minimum and maximum temperatures of  $-30.2^{\circ}\text{C}$  and  $-22.1^{\circ}\text{C}$ , respectively.

Figure 6. Air temperature measurements from eight sensors temporarily installed around the exterior of the South Pole Elevated Station during the lidar/TIR survey. See Appendix B for placement locations. Variation in temperatures is due to sensor location and the effects of solar exposure and winds.

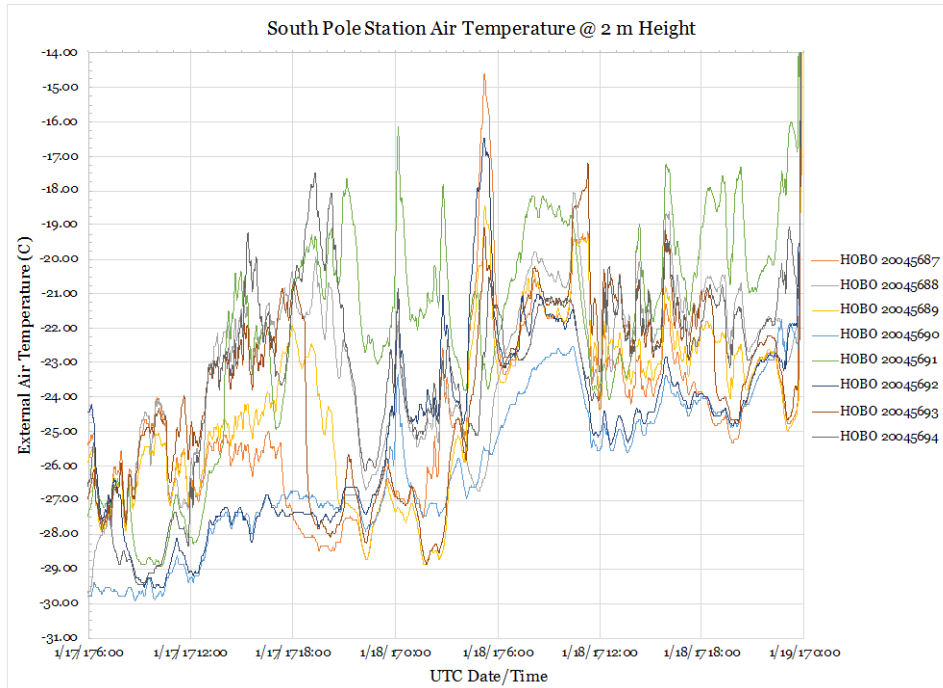


Figure 7. Plot of air temperature measurements for 17–19 January 2017 from the South Pole Observatory meteorological station, taken from 2 m above the snow surface. A minimum temperature of  $-30.2^{\circ}\text{C}$  occurred in the early morning of 17 January, and a maximum temperature of  $-22.1^{\circ}\text{C}$  occurred mid-morning on 18 January.

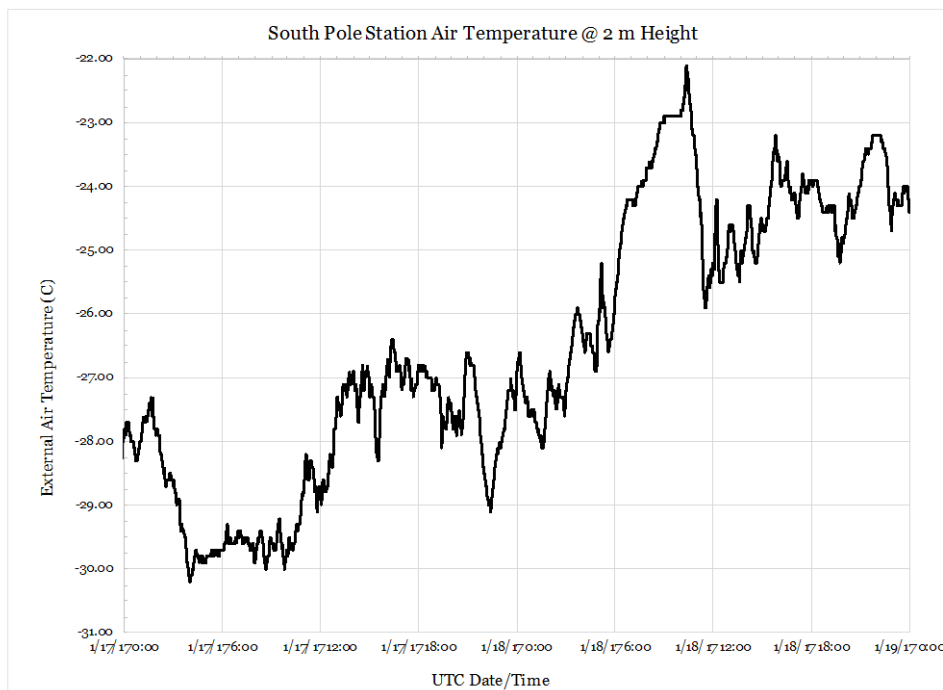
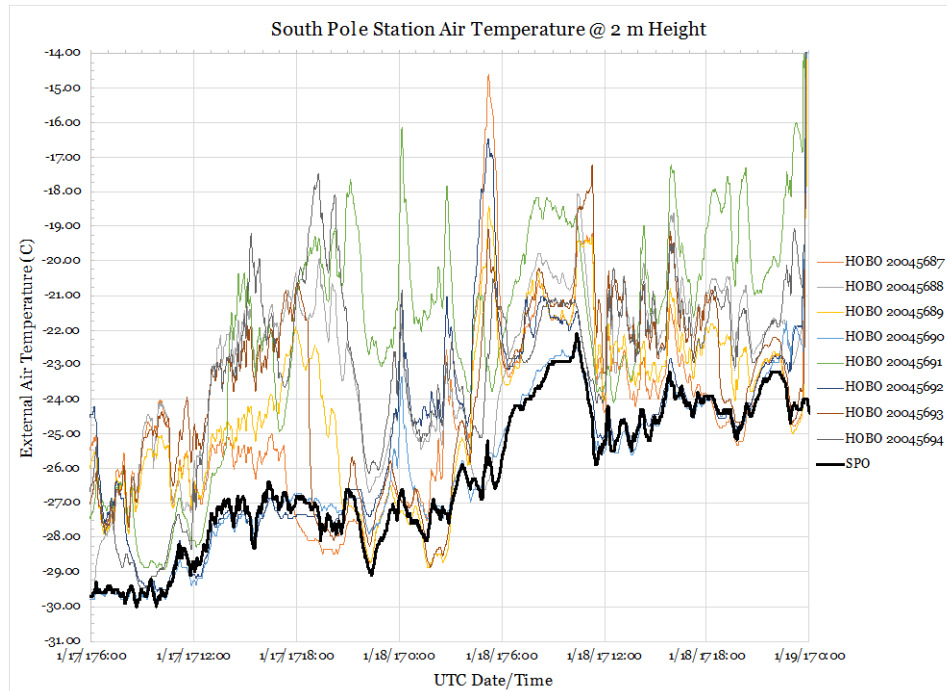


Figure 8 compares the temporary air temperature sensor measurements with the SPO data. The SPO data agree well with nearby HOBO air temperature sensors.

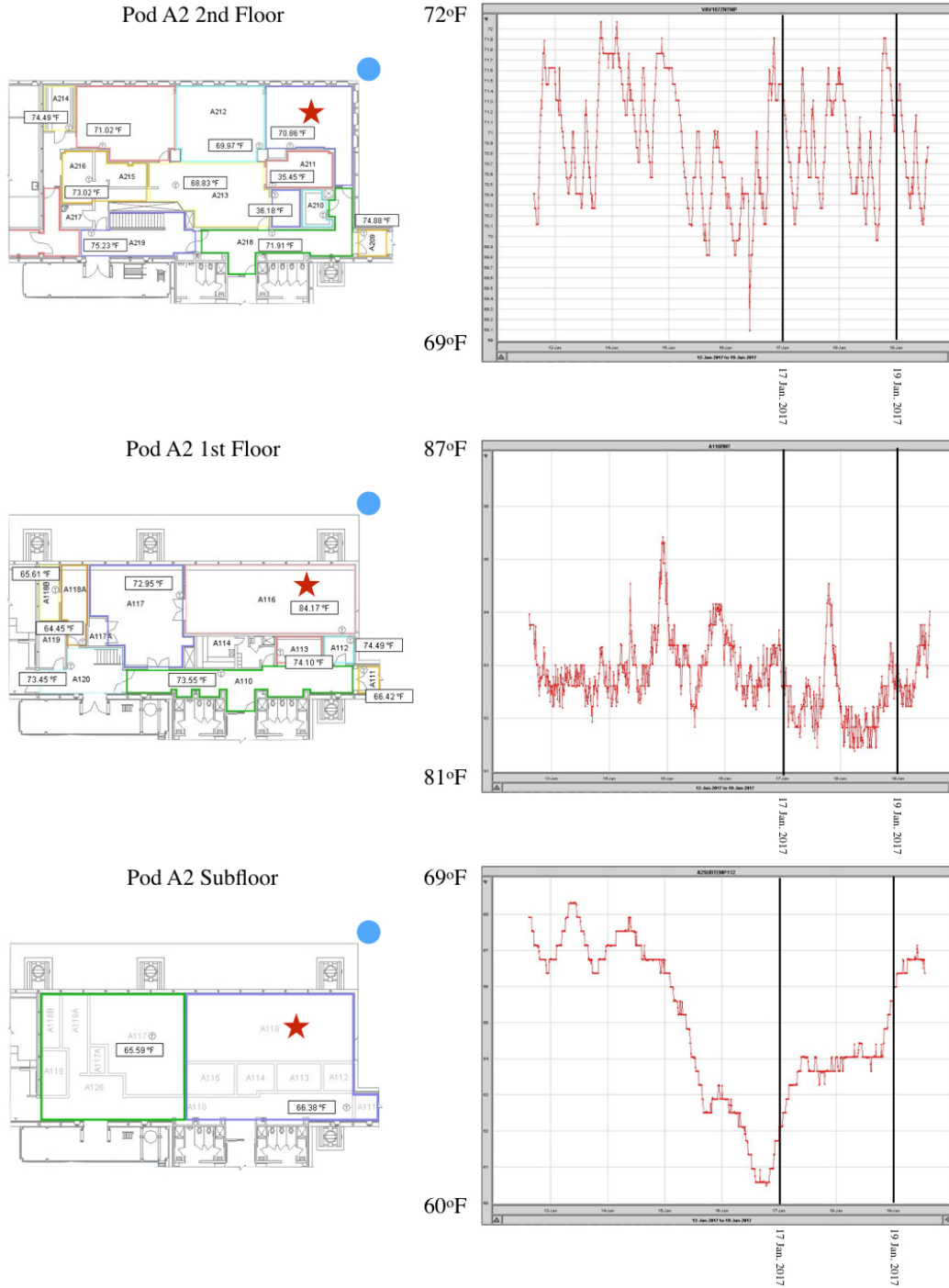
Figure 8. Plot of air temperature measurements for 17–19 January 2017 from all HOBO air temperature sensors (*color lines*) and the South Pole Observatory meteorological station (*black line*). Variations occur likely due to differences in location and thus atmospheric conditions.



### 3.2 Interior measurements

Given that the Elevated Station has environment monitoring sensors, including for air temperature, distributed throughout the building, we leveraged these data for use in measuring the thermal gradient between interior air temperatures and exterior surface temperatures. Figure 9 provides a sampling of these air temperature data along with a measurement location map. These data are used for reference where any thermal anomalies are identified in the 3-D thermal model, as discussed in section 5, “Results and Discussion.”

Figure 9. Example of interior air temperature measurements logged in Pod A2 of the Elevated Station (second, first, and subfloors). The *red stars* indicate the locations of temperature measurements plotted to the right of the floorplans. The *blue dots* indicates the location of the nearest external air temperature sensor (sensor 20045687).



### 3.3 GNSS control survey

To account for the absolute location and orientation of the Elevated Station with respect to a global coordinate system and to provide a baseline 3-D dataset that may be leveraged in future studies for spatial comparison (e.g., station motion and settlement observations), we performed a GNSS control survey. This process, referred to as georeferencing, was completed for the South Pole Station lidar/TIR survey by collecting RTK survey measurements of temporary reflectors placed in the scanner's FOV (Figure 10). "Data Processing" section discusses this process of georeferencing. We used a Trimble R8 system provided by the Station surveying team.

Figure 10. A 10 cm cylinder reflector setup during the South Pole lidar/TIR survey. The reflectors, with 10 cm height/diameter dimensions, provide reference coordinates used to tie the 3-D model to a global coordinate system.



A single RTK survey was completed for the South Pole survey as it is necessary to have only one lidar scan with the reflectors visible to georeference the entire dataset. The reflectors are 10 cm height/diameter cylinders covered in a reflective tape that is easily identified within a reflectance-colored point cloud. Four reflectors were distributed around scan position 22 and were surveyed on 19 January 2017 and had a height offset of the GNSS antenna applied to log the centroid of each reflector cylinder (Figure 11). Reference Figure 5 and Appendix B for scan position 22, GNSS base station, and reflector locations. We then collected high-resolution "tiepoint scans" during the lidar/TIR data acquisition procedure for scan position 22 and used them to precisely fit the point cloud to the UPS South coordinate system.

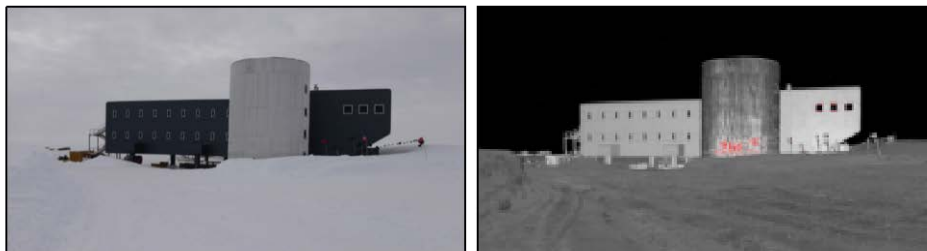
Figure 11. A 10 cm reflector cylinder with Trimble R8 antenna setup, highlighting the need to apply a height offset from the antenna measurement point to the cylinder centroid.



### 3.4 Handheld electro-optical imagery

While the reflectance-colored 3-D model derived from the lidar scanner provides sufficient distinction between differing surfaces, it is still beneficial to capture true-color images to assist in identifying specific building materials (Figure 12). Using a Nikon D800 DSLR with a 14–24 mm lens, we collected handheld electro-optical imagery at each scan position and for areas on the Elevated Station exterior identified with either damage or thermal deficiencies. Appendix B documents the position of each electro-optical imagery collection location. The image-naming convention is *South\_Pole\_EO\_Pos\_(scan position)\_xxx.JPG*, and all images have been delivered to NSF.

Figure 12. Electro-optical image (*left*) captured from scan position 20 compared to the reflectance-colored 3-D model (*right*), highlighting the utility of capturing true-color images in conjunction with the lidar/TIR data acquisition. The electro-optical imagery is helpful in identifying specific building and infrastructure materials and for providing visual context of the survey area.



### 3.5 Lidar/TIR system

The lidar/TIR system includes a Riegl VZ-1000 laser scanner; InfraTec VarioCAM HD thermal infrared camera; and for extreme cold temperature operations, a custom thermal jacket to maintain minimum operating temperatures for the lidar and TIR sensors (Figure 13). The system was mounted to a fiberglass survey tripod, which is both lightweight and less prone to thermal expansion/contraction compared to similar metal tripods. External batteries typically used for powering the system would have experienced dramatically reduced performance due to cold temperatures at the South Pole. Additionally, the thermal jacket requires 110VAC power; therefore, a portable generator (Honda EU2000) supplied by Station management was used to power both the lidar/TIR system and the thermal jacket (Figure 13). The generator, housed inside an insulated enclosure to retain heat, was towed behind a snowmobile between each scan position. Both lidar and TIR sensors were controlled by a ruggedized PC. The lidar sensor uses wireless communication while the TIR was connected via Ethernet cable to the PC. The PC was kept inside the operator's jacket between scan positions to maintain operating temperatures.

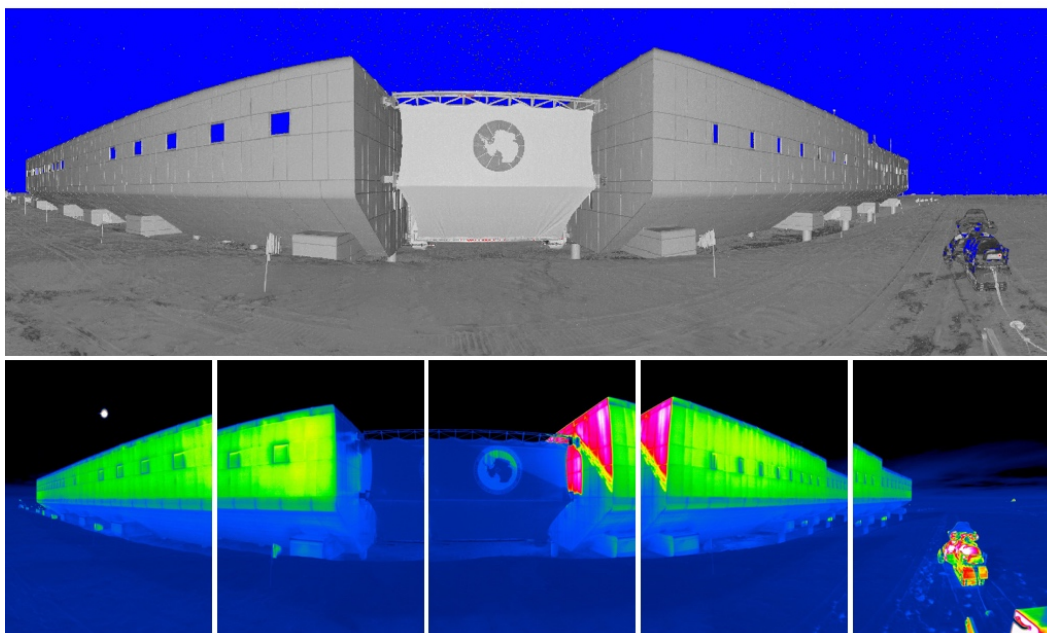
Figure 13. Author David Finnegan operating CRREL's lidar/TIR system at the South Pole Station. The thermal jacket was designed specifically for this survey, maintaining the minimum operating temperatures for both sensors. A generator, housed in the enclosure located on the snowmobile sled, provides power to both the system and the thermal jacket.



For each scan position, the survey tripod was placed on the snow with the tripod feet stomped down to better stabilize the system. We made efforts

to visually level the tripod; though, as a result of the data processing and georeferencing procedure, it was not necessary to perfectly level the system for each scan. At each scan position, we captured a high-resolution scan with the following scanning parameters: a  $100^\circ$  vertical  $\times$   $360^\circ$  horizontal FOV, a  $0.03^\circ$  angular increment (both vertically and horizontally), and a 300 kHz pulse repetition rate. The range from scanner position to target building surface varied but was typically 5–10 m, with longer stand-off distances for scan positions 15–22. These scan parameters resulted in roughly 8–28-million points/scan, with centimeter- to subcentimeter-scale point spacing on the building surface. At the conclusion of each lidar scan, we captured TIR images with a  $40^\circ$  horizontal overlap to ensure total coverage of the scan area. Figure 14 displays both the high-resolution lidar scan and the set of TIR images collected from a scan position. Detailed acquisition procedures are documented in Appendix C.

Figure 14. Example data from scan position 3. *Top*: 2-D view of lidar data, colored by surface reflectance. More reflective surfaces backscatter stronger laser returns. *Bottom*: Set of TIR images collected, colored by a  $-45^\circ\text{C}$  to  $-5^\circ\text{C}$  color scale. A 40% overlap between subsequent images is shown.



Because of line-of-sight limitations of both sensors and the complicated building footprint, 22 scan positions were required to capture the exterior of the Elevated Station. While we made every effort to minimize shadowed areas and thus data gaps, some sections of the building were obstructed by ground vehicles, drifted snow, exterior infrastructure, and scanner posi-

tion limitations. We collected these data in four acquisition sessions to optimize atmospheric conditions (solar exposure, blowing snow/precipitation, etc.), to reduce on-site personnel activity, and to allow the survey team and the system to warm up. Appendix D provides a detailed log of each scan position, including lidar and TIR acquisition times, building focus area, atmospheric observations (air temperature and relative humidity), and scanning notes.

## 4 Data Processing

### 4.1 Lidar scans registration and georeferencing

Because line-of-sight limitations and the building's exterior complexity (multiple pods and facets), it was necessary to collect lidar/TIR data from 22 separate scan positions. Further, to produce a collective 3-D model requires registration and georeferencing of these disparate datasets. Registration is the process of tying individual point clouds to each other whereas georeferencing refers to the process of tying the point clouds to a global coordinate system. For the South Pole Station survey, these processes were conducted simultaneously.

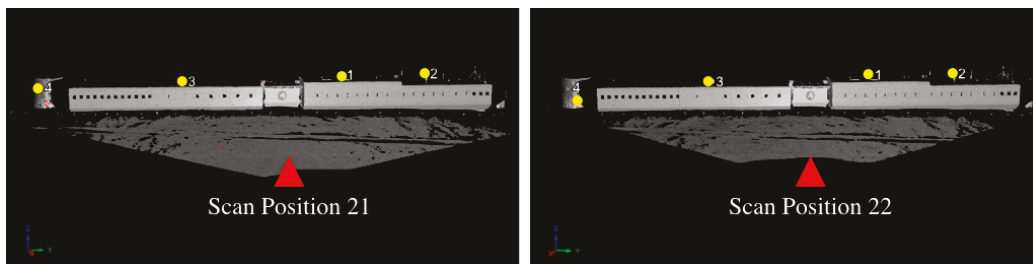
Using the four 10 cm cylinder reflectors and the GNSS RTK survey data, scan position 22 was tied to the UPS South coordinate system. Because the reflectors were scanned from scan position 22, the centroid XYZ coordinates ( $X$  = longitude,  $Y$  = latitude,  $Z$  = elevation) of each cylinder was measured and identifiable within the point cloud. The XYZ coordinates measured by the GNSS survey were then assigned to the reflector positions in the point cloud. This established the baseline georeferenced scan to which all remaining scans are registered.

The subsequent scans (scan positions 1–21) were tied to the baseline georeferenced scan (22) through a two-step process: coarse registration and Multi-Station Adjustment (MSA). Coarse registration involves identifying a minimum of four common points between overlapping scans to roughly align the point clouds together. The baseline scan's position/orientation is locked while the unregistered scan's position/orientation is allowed to be modified. For example, scan positions 22 and 21 were acquired from roughly the same physical location and therefore have many similar point measurements in which to identify common points (Figure 15). This process, while helpful in roughly aligning multiple point clouds, is limited by the user's ability to select common points and results in typical positional errors on the centimeter-to-meter scale.

MSA uses a planar filter algorithm that identifies planar features within each point cloud and then iteratively aligns the unregistered scan data to the baseline point cloud. This process involves initial user input, including the minimum number of points required to define a plane and the minimum and maximum search radius between two point clouds to identify

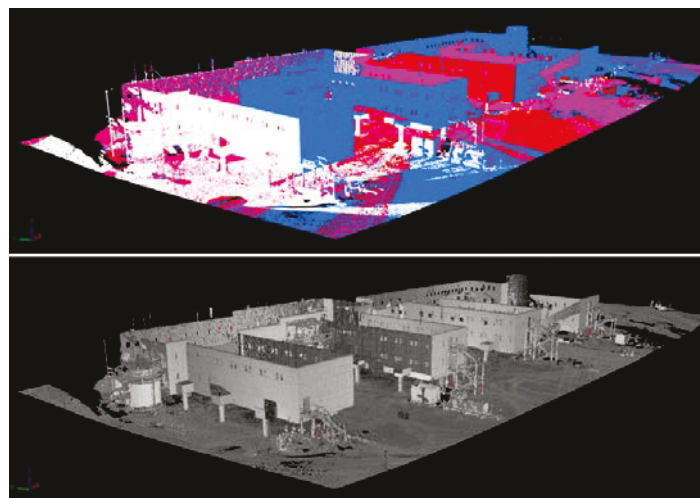
similar planar features. The calculated planes from different scans are then aligned, resulting in a typical positional error between multiple point clouds in the subcentimeter scale. Details and step-by-step processing notes are found in Appendix E.

Figure 15. Visualization of the coarse registration process in which an unregistered scan is roughly aligned to a registered, georeferenced baseline scan. Scan position 22 (*right*) was tied to the UPS South coordinate system using reflectors and the GNSS RTK survey. Scan position 21 (*left*) was captured from a similar position as 22 and therefore has significant overlap. Common features are manually identified between each point cloud (yellow dots), and scan position 21's position/orientation is subsequently modified.



Beginning with scan position 22 as the baseline scan, all subsequent scans were coarse registered / MSA processed in the following order, dictated by the quantity of overlapping surfaces between neighboring scans: 003, 002, 004, 005, 001, 006, 007, 015, 016, 017, 018, 019, 011, 020, 014, 008, 013, 009, 009b, 012, and 010. After MSA processing was complete, the registration and georeferencing processes were complete, and the point clouds may be viewed as a complete 3-D model (Figure 16).

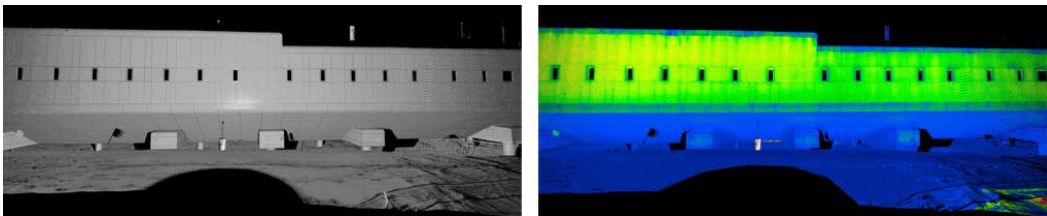
Figure 16. Lidar data of the Elevated Station was collected from 22 different scan positions. Each resulting point cloud covered a portion of the Station. The *top* image shows eight of these point clouds, colored by scan position. After registration/georeferencing, the individual scans combine to create a complete 3-D model of the Station (*bottom*).



## 4.2 Thermal infrared radiometric value registration

Each scan position has associated TIR imagery covering the same FOV as the lidar point cloud. The temperature values measured by the TIR sensor can be mapped and assigned to each individual point measurement (Figure 17). To complete this task, a camera calibration associated with the TIR detector and lens distortion and a camera-mounting calibration associated with the position/orientation of the TIR with respect to the lidar origin were created in Riegl's RiSCAN Pro software by the survey team. This allows each pixel of the thermal image to be assigned to each individual lidar measurement based on the scan angle of the laser. For each point cloud, the thermal value is written to the LAS file format *GPS Time* field for dynamic visualization in 3-D point cloud viewing applications. In addition, a continuous color scale from blue to red, based on temperature, is used to set the red-green-blue (*RGB*) fields in the LAS file. This is useful for 3-D model viewers that are unable to colorize point clouds by their *GPS Time* values. For further discussion on attributing thermal values to the point clouds, see Appendix F.

Figure 17. A 3-D model captured from scan position 4 colored by surface reflectance (*left*) and temperature (*right*). Mapping the TIR imagery onto the 3-D model visually represents thermal variations.



## 4.3 Data products

The data processing steps produced specific data products. Each scan position provides the following deliverables:

1. Full-resolution georeferenced point clouds from each scan position, with reflectance and temperature values assigned to each point measurement—Temperature values are located in the *GPS Time* field in the LAS-zipped (.laz) file format. RGB values represent a fixed-scale temperature colorization. *Naming convention: YYYYMMDD\_HHMMSS.laz*
2. A 2 cm subsampled, georeferenced point cloud from each scan position, with reflectance and temperature values assigned to each point measurement—Octree filter subsampling is applied to the point cloud, averaging all

- point values (XYZ, reflectance, and temperature) into 2 cm cubes. Temperature values are located in the *GPS Time* field in the LAS-zipped (.laz) file format. RGB values represent a fixed-scale temperature colorization.  
*Naming convention: YYYYMMDD\_HHMMSS-2cmSample.laz*
3. A 2 cm subsampled, georeferenced point cloud of all scan positions combined, with reflectance and temperature values assigned to each point measurement—Octree filter subsampling is applied to the point cloud, averaging all point values (XYZ, reflectance, and temperature) into 2 cm cubes. Temperature values are located in the *GPS Time* field in the LAS-zipped (.laz) file format. RGB values represent a fixed-scale temperature colorization. Naming convention: *2017-01-SouthPole-2cmSample.laz*
  4. Set of panoramic TIR images in both proprietary InfraTec file format (.irb) and fixed color scale .jpg file format—*Naming convention: ScanPos(XXX) – Image(XXX).irb/.jpg*
  5. Set of panoramic electro-optical images in .jpg file format taken from each scan position location and any detail images of observed exterior damage or thermal deficiency—*Naming Convention: South\_Pole\_EO\_Pos\_(scan position)\_xxx.jpg*

## 5 Results and Discussion

### 5.1 Solar-exposure limitations

Because the lidar scanner measures only 1550 nm wavelength backscattered light transmitted by the laser source, ambient light does not significantly affect the quality of data or performance of the sensor. In contrast, the TIR measures light in the 7.5–14  $\mu\text{m}$  wavelength range and is therefore affected by the presence of ambient light and reflected solar radiation, thermal emission from the temperature of the shaded areas of the building increasing due to recent solar radiation, and thermal emission based on thermal envelope deficiencies. Specifically, sections of the building receiving direct sunlight during the time of acquisition alter the radiometric measurement by the TIR sensor by measuring reflected solar radiation. While thermal variations within the solar-exposed area are still measurable, the increase in apparent temperature due to incident solar radiation makes qualitative analysis difficult when both shaded and unshaded regions are present. This is due to the larger temperature domain and sharp variations in apparent temperature over short spatial distances (Figure 18). Given that there was full 24-hour daylight during the field campaign, there are portions of the Elevated Station exterior that always had some direct sunlight during image acquisition. However, these sun-exposed sections may be analyzed using a different set of temperature scales, thus allowing for thermal variations in the exterior to be identified, yet not directly compared to shaded regions (Figure 19). For the results analysis, building surfaces are broken into two groups: solar exposed and shaded.

Figure 18. A 3-D thermal model colored by temperature ( $-45^{\circ}\text{C}$  to  $-5^{\circ}\text{C}$ ) taken during a period with direct sun exposure on a portion of the Elevated Station exterior. Note the high-temperature surfaces (*white*) appear saturated with this temperature scale.

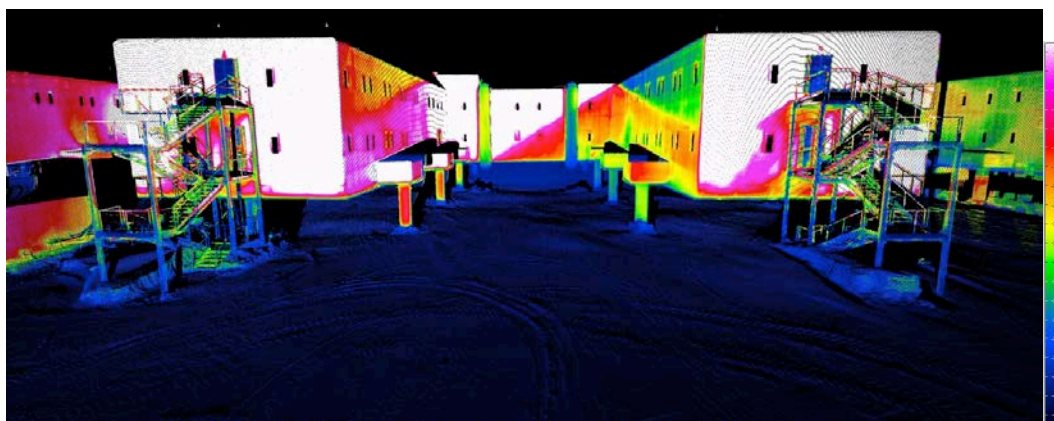
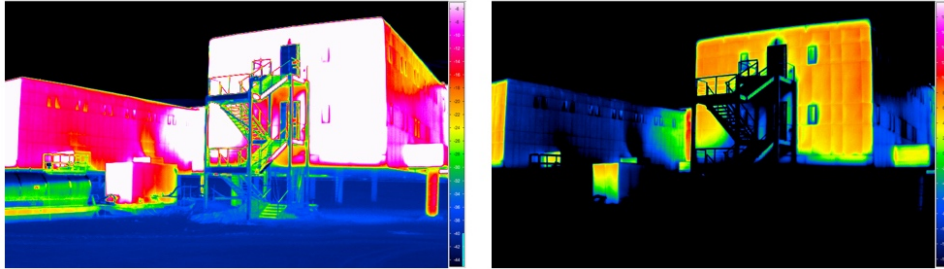


Figure 19. A thermal image of wing B1 taken from scan position 17. Because of direct solar exposure on the end wall, the thermal values are elevated, reducing the level of detail visible across a wider temperature scale of  $-45^{\circ}\text{C}$  to  $-5^{\circ}\text{C}$  (*left*). By altering the temperature scale of the thermal image ( $-15^{\circ}\text{C}$  to  $20^{\circ}\text{C}$ ) to optimize detail in the solar-exposed sections, relative thermal differences are apparent (*right*). Conversely, lower temperatures (snow and shaded surfaces) lose definition with the solar-exposed temperature scale.



## 5.2 Exterior surface thermal analysis

The 3-D thermal model can be divided by building wing and aspect. For the purposes of analysis, we will use a grid north orientation, where the north side of the building refers to Wings A2, A3, B2, and B3 and south refers to Pods A and B (Wings A1, A4, B1, and B4). While some thermal deficiencies exist, overall the Elevated Station's thermal envelope appears to be both tight and effective. When comparing these data to lidar/TIR data collected from Palmer Station, Antarctica, in 2015, it is readily apparent that the buildings there, excluding the recently built Terralab, suffer from significant thermal envelope degradation (Figure 20). This provides both reference and validation that the building material and construction techniques and implementation used in the design of the Elevated Station are sound and effective. Figures 21–45 identify any thermal deficiencies, if observed, with accompanying detail imagery.

Figure 20. Comparison of Palmer Station and South Pole Station lidar/TIR results. *Left*: Palmer Station Biolab,  $5^{\circ}\text{C}$  to  $-15^{\circ}\text{C}$  scale. *Middle*: Palmer Station GWR (garage, warehouse, and recreation) building,  $5^{\circ}\text{C}$  to  $-15^{\circ}\text{C}$  scale. *Right*: South Pole Station Wing B3 North,  $5^{\circ}\text{C}$  to  $-45^{\circ}\text{C}$  scale. While the temperature scales are different due to differences in air temperature from each survey, the thermal deficiencies in the Palmer Station buildings are obvious while South Pole Station displays a significantly more uniform temperature scale.



Figure 21. A 3-D thermal model of Wings A2/A3. Overall the exterior surface on the north side of Wings A2 and A3 is at a consistent temperature with little heat loss emanating from the windows. Structural insulated panels (SIP) and trim are easily identified by the consistent lower temperature of the trim. A detached piece of trim was identified by its lower temperature compared to adjacent, attached trim. The overhanging, down-facing exterior portion of the Pod A subfloor is consistently lower in temperature, likely due to unused crawl space and proximity to the snow surface. *Top left:* Focus section highlighted in red on the Elevated Station map. *Bottom:* North side of Wings A2 and A3,  $-40^{\circ}\text{C}$  to  $-15^{\circ}\text{C}$  scale. Temperature differences between SIP and trim are visible. The section with detached trim is outlined in red. *Top right:* Underside view of a piece of detached trim identified initially by its lower temperature.

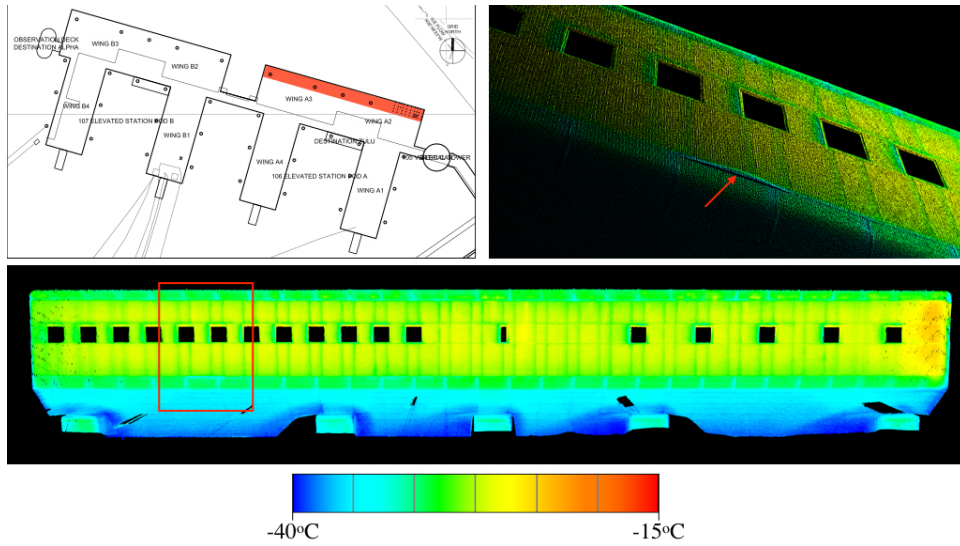


Figure 22. A 3-D thermal model of Wing A3 West. *Top left:* Focus section highlighted in red on the Elevated Station map. *Bottom:* Wing A3 West at a  $-40^{\circ}\text{C}$  to  $-15^{\circ}\text{C}$  scale.

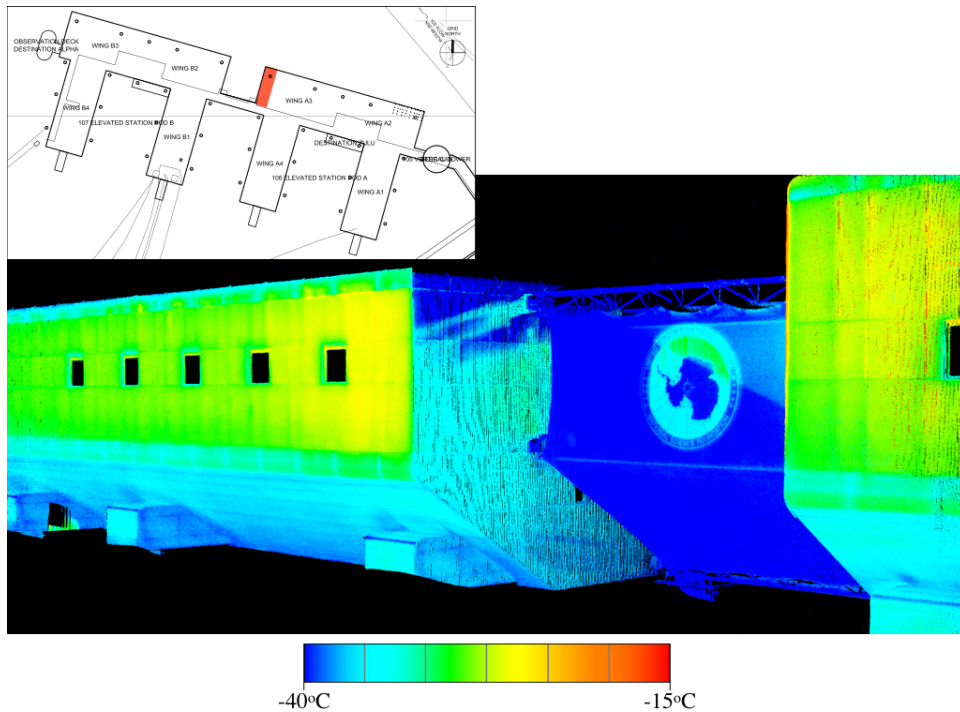


Figure 23. A 3-D thermal model of Wing B2 East. While the north facing sides of Wing A3 and B2 display consistent temperatures, the East face of Wing B2 is partially exposed to direct sunlight, causing an area of higher temperatures. Differences between SIP and trim are still observable. *Top left:* Focus section highlighted in red on the Elevated Station map. *Bottom:* Wing B2 East at a  $-40^{\circ}\text{C}$  to  $-5^{\circ}\text{C}$  scale. Solar-exposed surfaces on the upper right side of Wing B2 East result in significantly higher radiometric measurements with the TIR camera (red/orange sections).

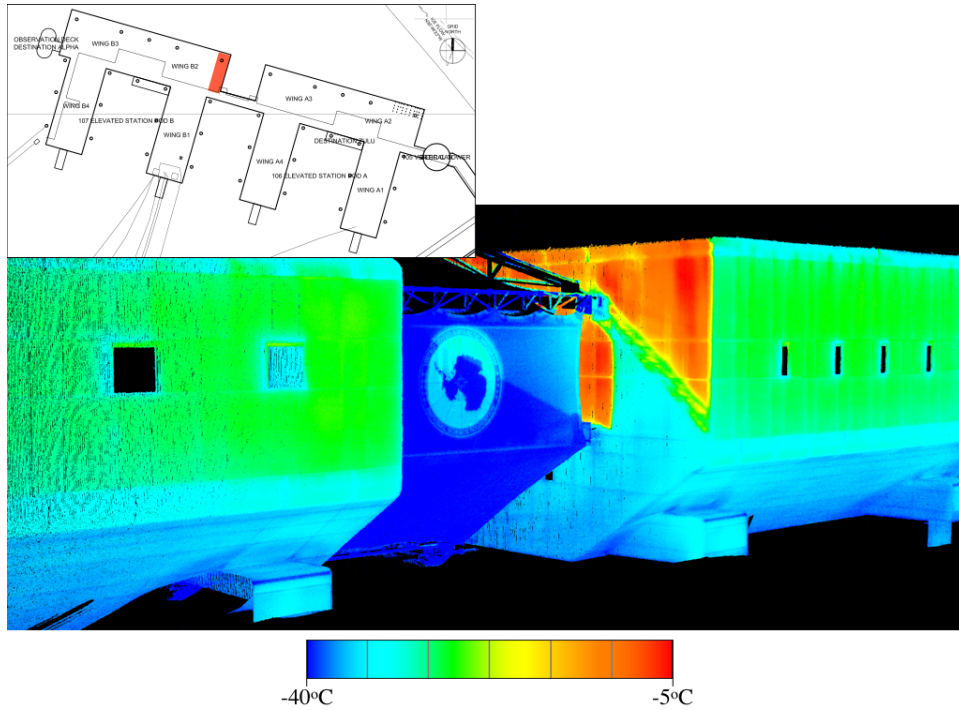


Figure 24. A 3-D thermal model of Wing B2 North. *Top left:* Focus section highlighted in red on the Elevated Station map. *Bottom:* Wing B2 North at a  $-40^{\circ}\text{C}$  to  $-15^{\circ}\text{C}$  scale.

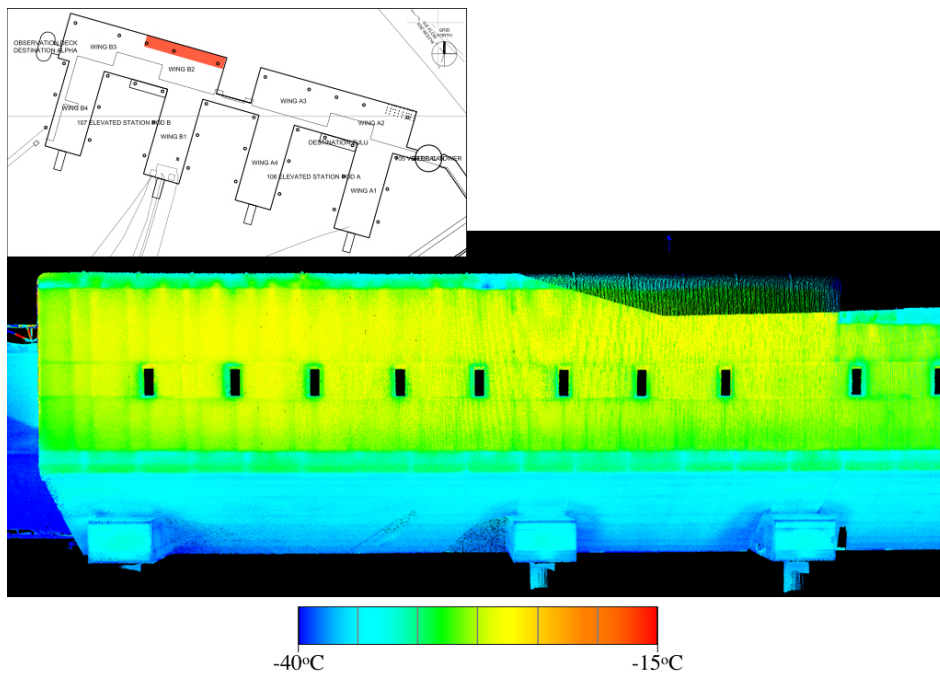


Figure 25. A 3-D thermal model of Wing B3 North. On Wing B3 North, two areas of interest were identified by using the thermal values in combination with the 3-D point cloud. First, an area of slightly detached SIP trim is visible above and to the left of the fourth window from the right. Fig. 26 shows an electro-optical image of this area. Likewise, two pieces of vertical trim towards the right side of the wall are detached, as noticed through lower temperatures. *Top left*: Focus section highlighted in red on the Elevated Station map. *Bottom*: Wing B3 North at a  $-40^{\circ}\text{C}$  to  $-20^{\circ}\text{C}$  scale. Trim detachment was identified on the fourth window from the right (*red square*) and on two vertical trim pieces (*top right*).

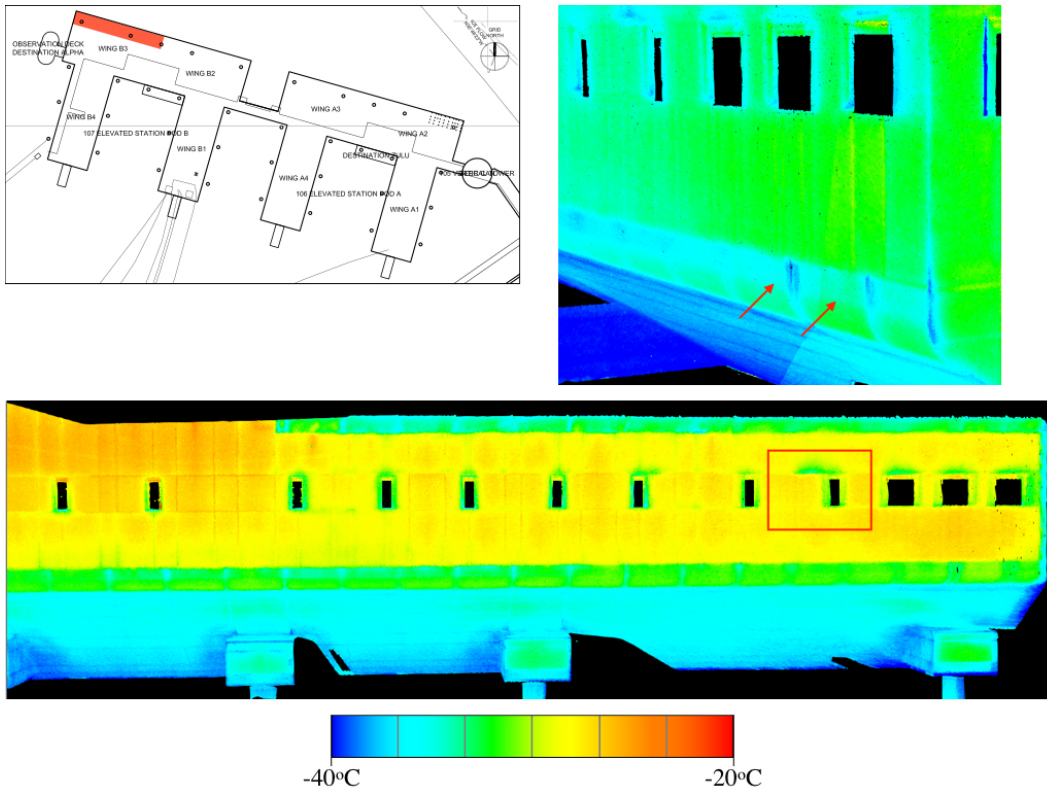


Figure 26. Wing B3 North SIP trim detachment. Temperature variation at SIP trim, allowing identification of trim fit issues and/or damage. The electro-optical image confirms the trim piece in question is dislodged from the SIPs.

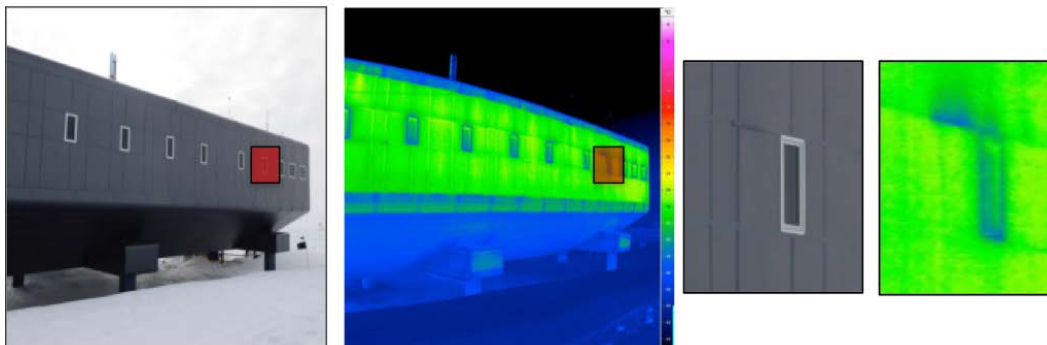


Figure 27. A 3-D thermal model of Wing B3 West and portion of Observation Deck Destination Alpha. *Top left:* Focus section highlighted in red on the Elevated Station map. *Bottom:* Wing B3 West at a  $-40^{\circ}\text{C}$  to  $-20^{\circ}\text{C}$  scale.

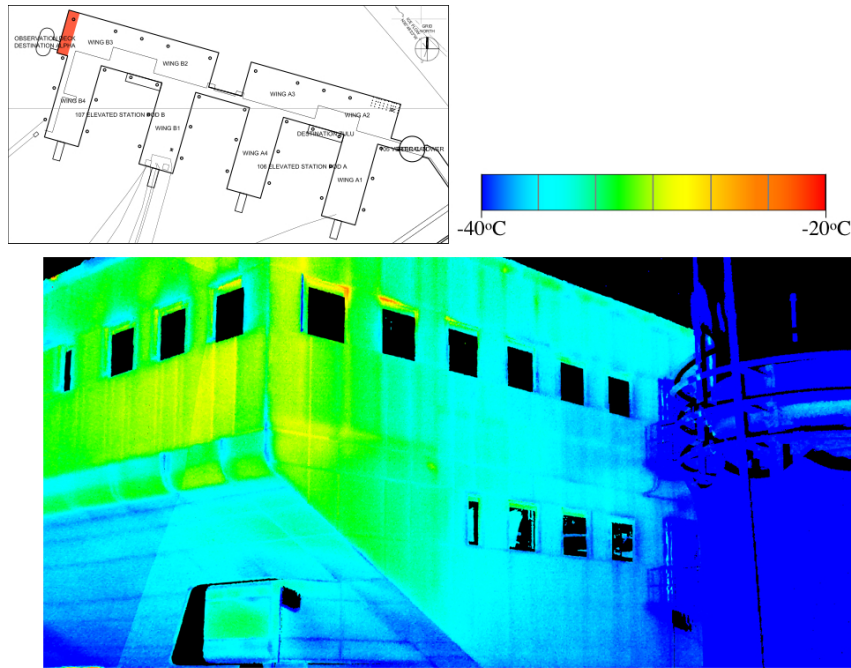


Figure 28. A 3-D thermal model of Wing B4 West. The second floor windows on Wing B4 West show signs of significant temperature differences. The interior temperatures of this section (the gymnasium) fluctuate between  $18^{\circ}\text{C}$  and  $20^{\circ}\text{C}$  throughout the lidar/TIR survey, so it is possible there was heat loss occurring from these windows. *Top left:* Focus section highlighted in red on the Elevated Station map. *Bottom:* Wing B4 West at a  $-35^{\circ}\text{C}$  to  $-5^{\circ}\text{C}$  scale. The red box indicates windows with high thermal gradients above and along the sides of the frames. *Top right:* Detail view of the windows in questions.

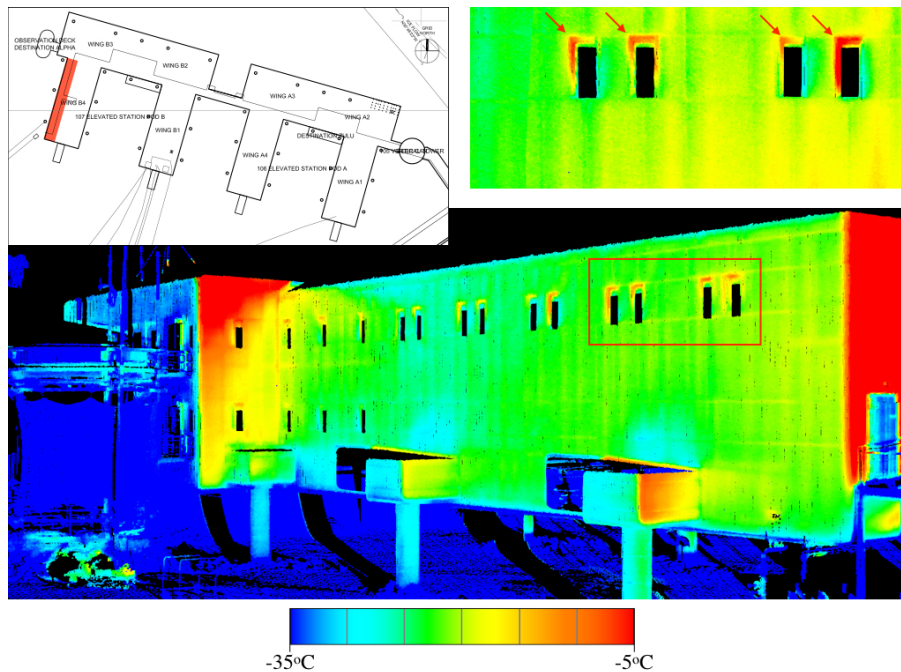


Figure 29. A 3-D thermal model of Wing B4 South. Because of direct solar exposure on the Wing B4 South external surface throughout our entire time on station, the TIR measurements are significantly higher than the unexposed sections. Increasing the color scale temperature values better shows relative temperature differences. Of note is the lack of any substantial heat loss from the first floor door, indicating that the doors, designed for industrial freezers, are performing well. *Top left:* Focus section highlighted in *red* on the Elevated Station map. *Bottom:* Wing B4 South at a  $-15^{\circ}\text{C}$  to  $15^{\circ}\text{C}$  scale. Because of direct solar exposure, all south-facing surfaces must be displayed with higher color scale temperatures to reveal relative surface-temperature differences. The *red arrow* highlights almost no heat loss emanating from the doorway.

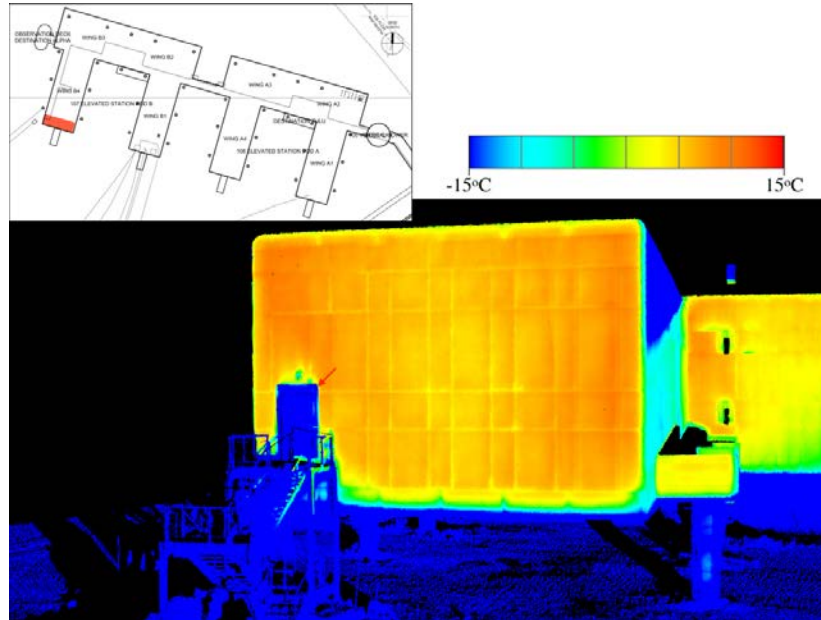


Figure 30. A 3-D thermal model of Wing B4 East. *Top left:* Focus section highlighted in *red* on the Elevated Station map. *Bottom:* Wing B4 South at a  $-15^{\circ}\text{C}$  to  $-5^{\circ}\text{C}$  scale. *Top:* Wing B4 South at a  $-40^{\circ}\text{C}$  to  $-10^{\circ}\text{C}$  scale

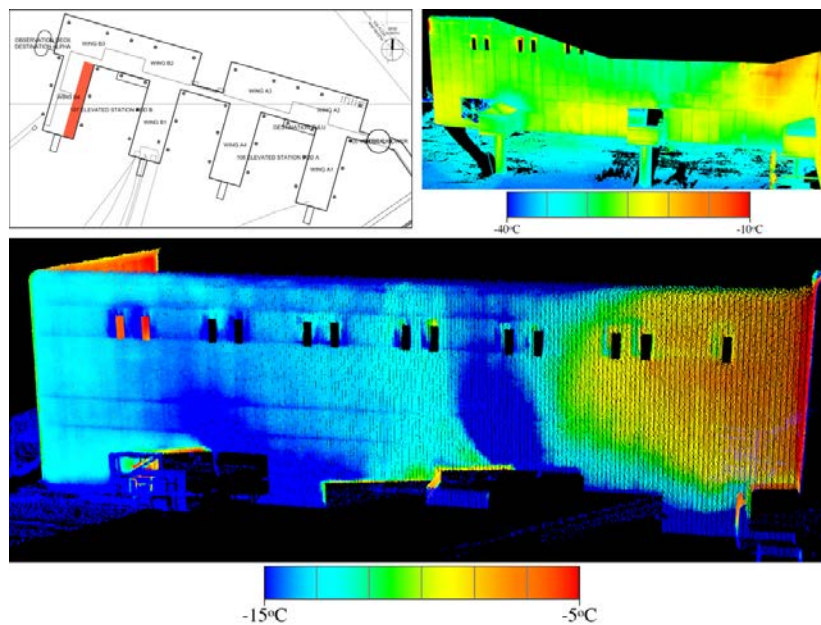


Figure 31. Wing B4 East. The four *red vertical rectangles* encompass areas of thermal bridging from the building frame structure, with measurements of up to 4 °C difference across the bridging sections. The enlarged window (*inset image*) identifies an area of heat loss of up to 20 °C difference (−29 °C to −9 °C). The windows located on Wing B4 West (Fig. 28), directly across from the highlighted window below, also show heat loss.

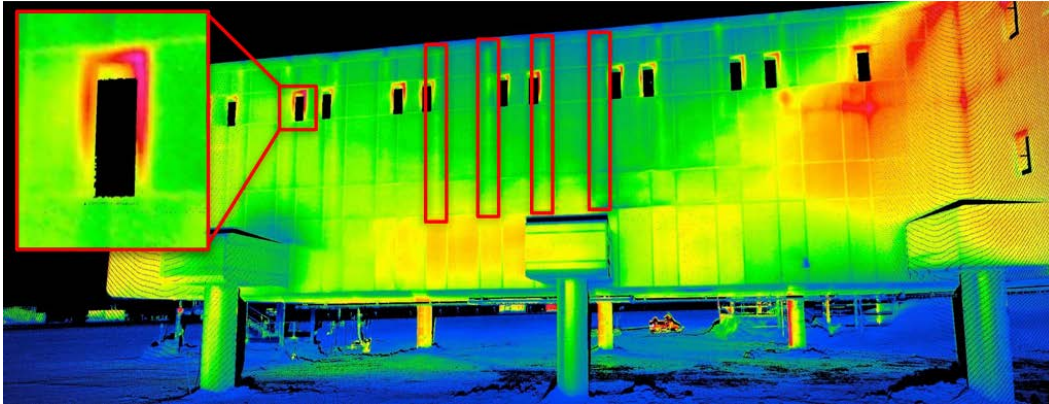


Figure 32. A 3-D thermal model of Wing B2/B3 South. *Top left:* Focus section highlighted in *red* on the Elevated Station map. *Bottom:* Wing B2/B3 South at a −45 °C to 20 °C scale. The temperature scale is wide due to areas of both exposed and unexposed to direct sunlight. A potential trim detachment was observed adjacent to the second floor left window on the B2/B3 South face, highlighted by the *red box*.

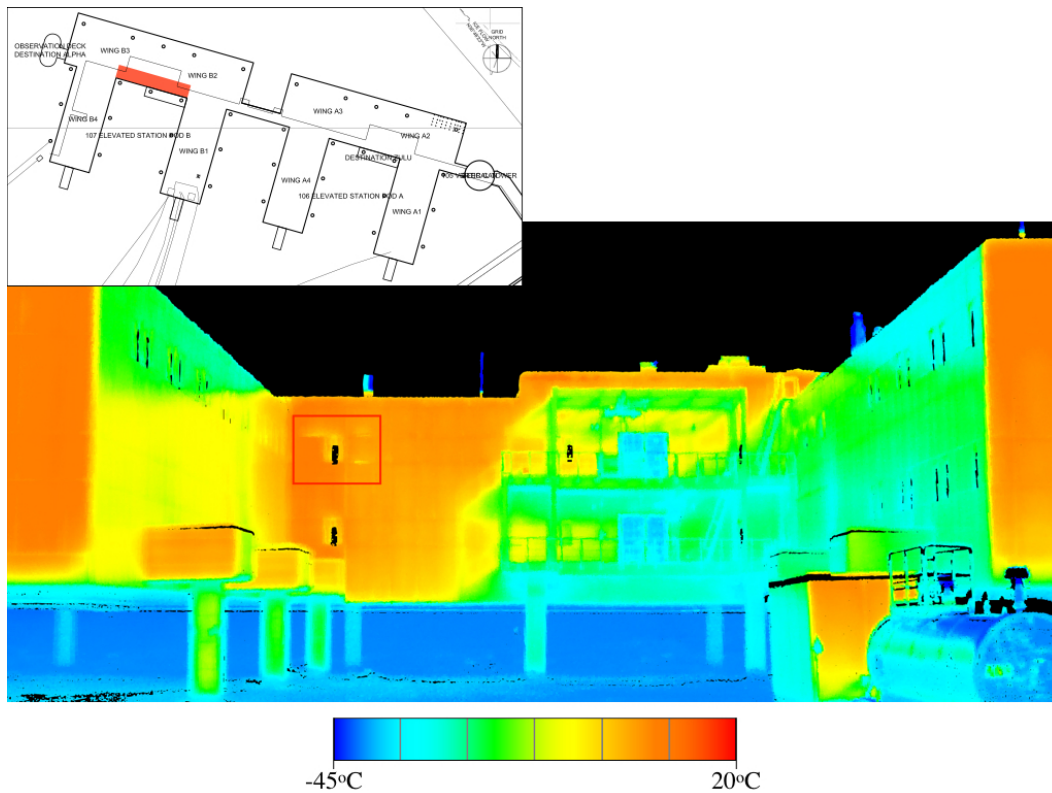


Figure 33. A 3-D thermal model of Wing B1 West. Significant thermal bridging, or a path of least resistance for heat to escape from the interior of the building, was observed and measured on most of the East and West faces of Wings A1, A4, B1, and B4. We posit that the thermal bridging is occurring from the building's internal frame and could potentially be avoided in future designs by ensuring there is overlapping insulation where the frame abuts the exterior walls. *Top left:* Focus section highlighted in *red* on the Elevated Station map. *Bottom:* Wing B1 West at a  $-40^{\circ}\text{C}$  to  $-10^{\circ}\text{C}$  scale. Significant thermal bridged was measured across the entire face, with a section highlighted by the *red box* and expanded for detail (*top right*). Note that these do not correlate with the SIP trim locations.

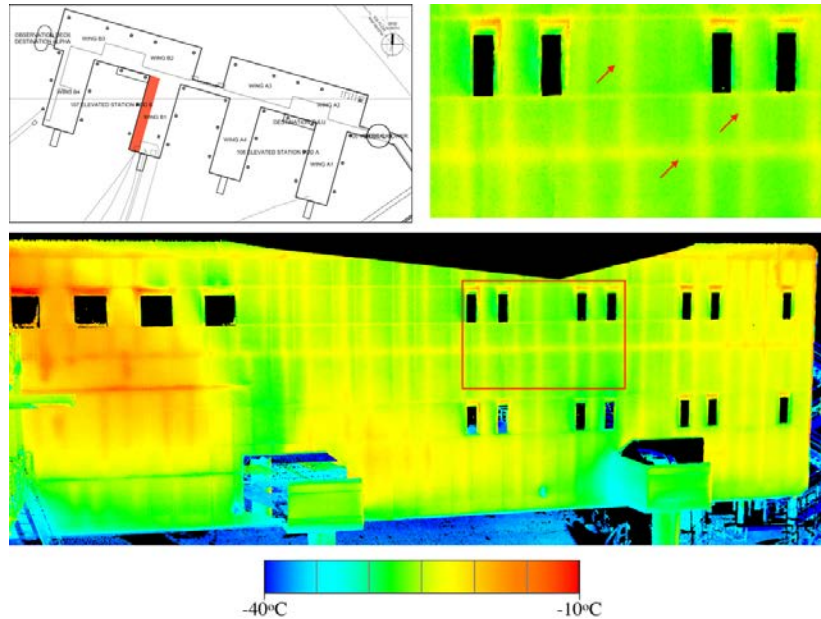


Figure 34. A 3-D thermal model of Wing B1 South. *Top left:* Focus section highlighted in *red* on the Elevated Station map. *Bottom:* Left and right views of Wing B4 South at a  $-15^{\circ}\text{C}$  to  $15^{\circ}\text{C}$  scale. Because of direct solar exposure, all south-facing surfaces must be displayed with higher color scale temperatures to reveal relative surface temperature differences.

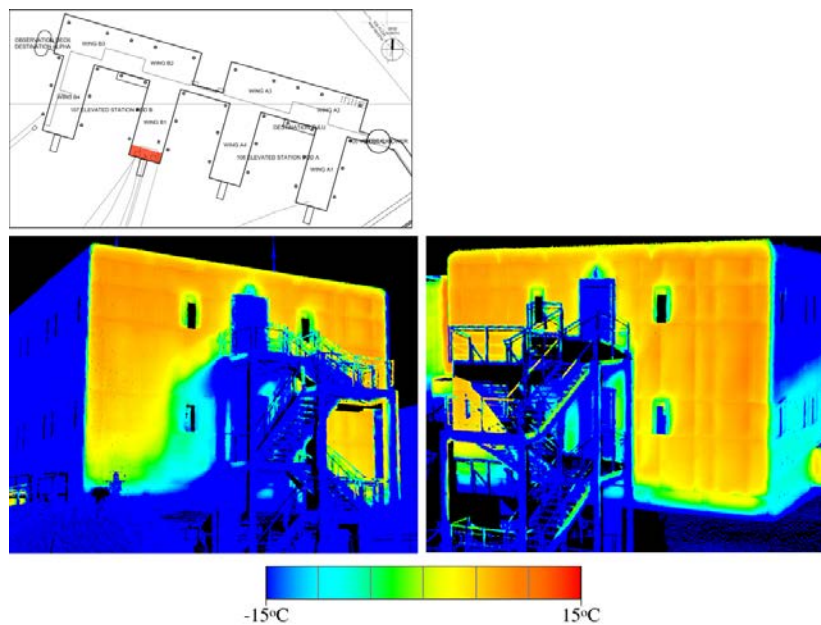


Figure 35. A 3-D thermal model of Wing B1 East. *Top left:* Focus section highlighted in red on the Elevated Station map. *Bottom:* Wing B1 East at a  $-40^{\circ}\text{C}$  to  $-15^{\circ}\text{C}$  scale. *Top right:* Detail of a generator exhaust vent at a  $-40^{\circ}\text{C}$  to  $20^{\circ}\text{C}$  scale.

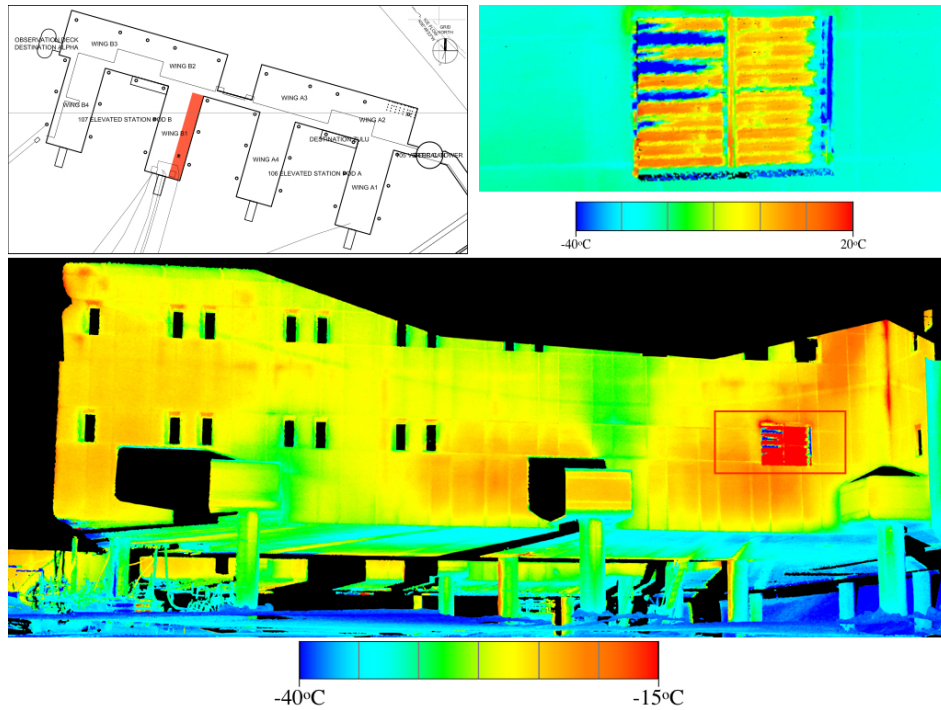


Figure 36. A 3-D thermal model of Pod A/B Connector South. *Top left:* Focus section highlighted in red on the Elevated Station map. *Bottom:* Pod A/B Connector South at a  $-40^{\circ}\text{C}$  to  $15^{\circ}\text{C}$  scale. No significant heat loss observed along the pod connection points.

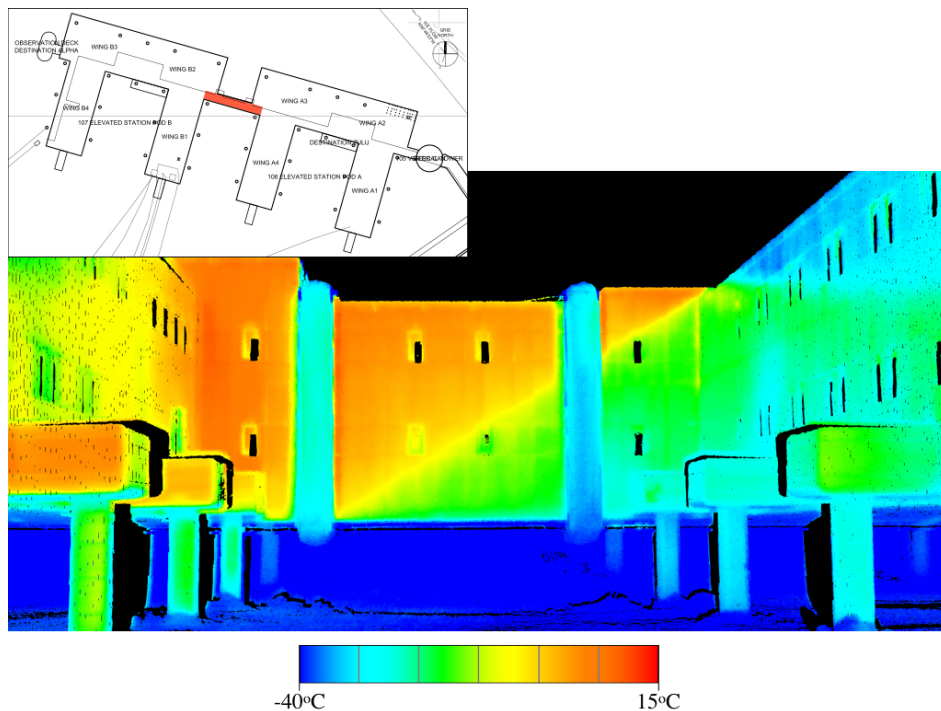


Figure 37. A 3-D thermal model of Wing A4 West. *Top left:* Focus section highlighted in red on the Elevated Station map. *Bottom:* Wing A4 West at a  $-40^{\circ}\text{C}$  to  $-10^{\circ}\text{C}$  scale. Thermal bridging and higher thermal gradients along the top windows are apparent.

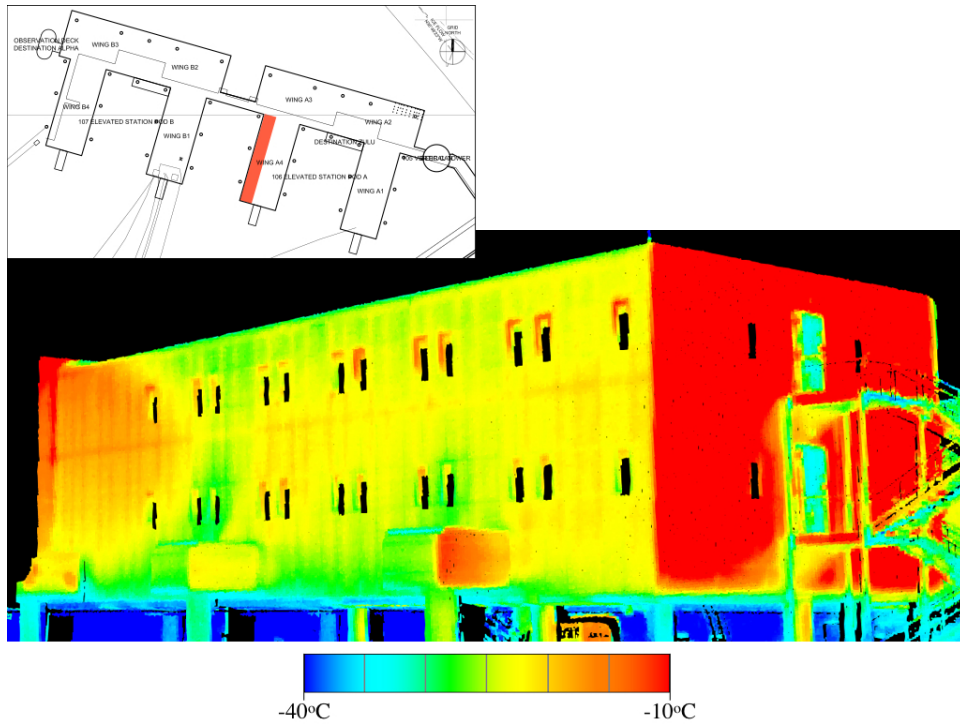


Figure 38. A 3-D thermal model of Wing A4 South. *Top left:* Focus section highlighted in red on the Elevated Station map. *Bottom:* Left and right views of Wing A4 South at a  $-15^{\circ}\text{C}$  to  $15^{\circ}\text{C}$  scale.

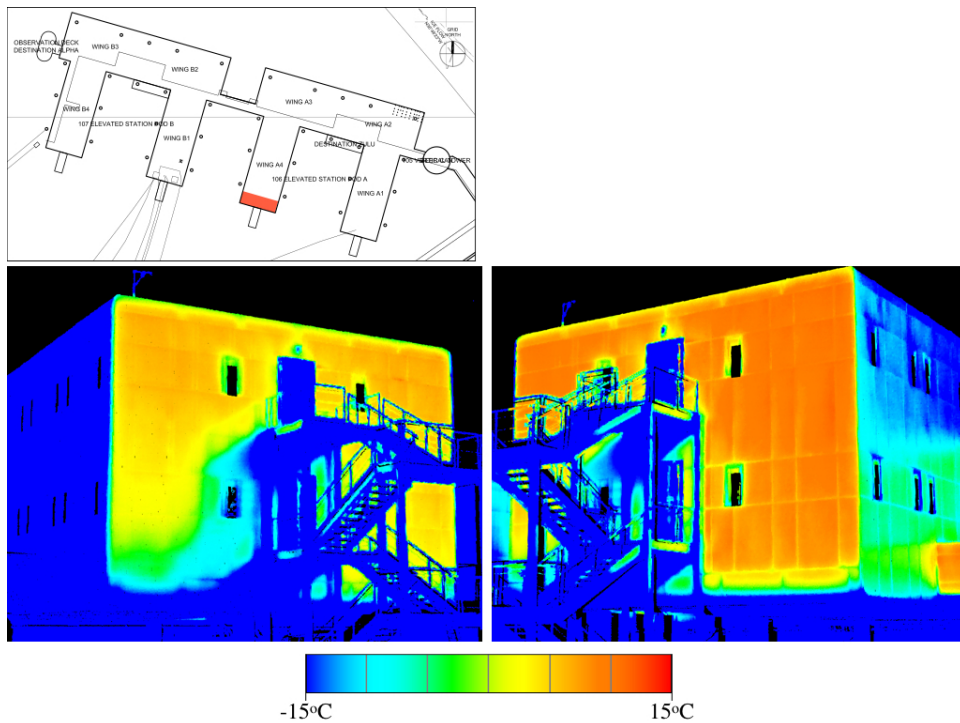


Figure 39. A 3-D thermal model of Wing A4 East. *Top left:* Focus section highlighted in *red* on the Elevated Station map. *Bottom:* Wing B1 East at a  $-40^{\circ}\text{C}$  to  $-10^{\circ}\text{C}$  scale. Areas of heat loss from windows are indicated by *red arrows*.

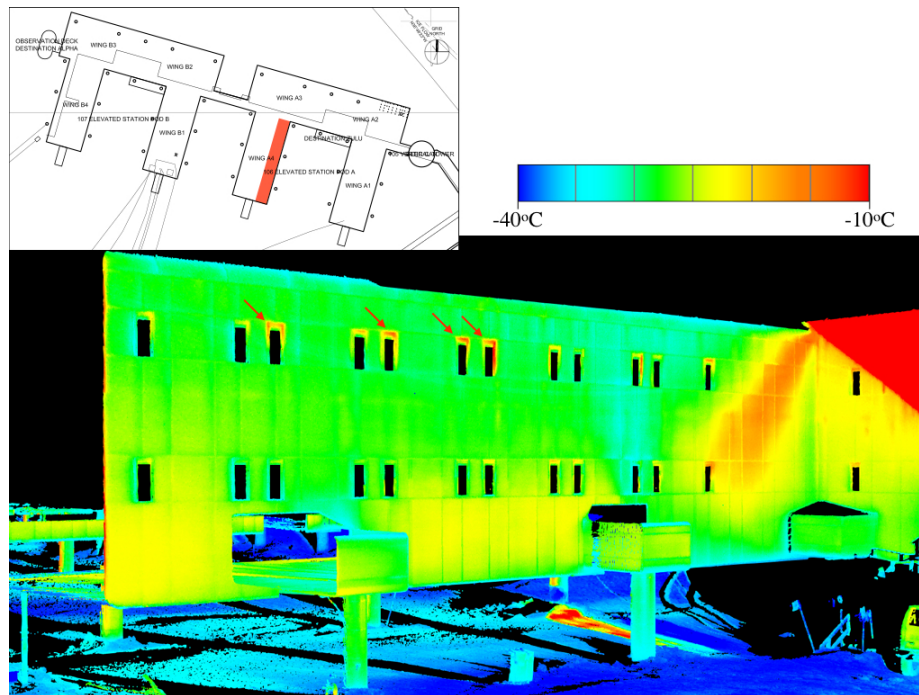


Figure 40. A 3-D thermal model of Wing A2/A3 South and Destination Zulu. *Top left:* Focus section highlighted in *red* on the Elevated Station map. *Bottom:* Wing A2/A3 South at a  $-40^{\circ}\text{C}$  to  $-15^{\circ}\text{C}$  scale. The transition line from the solar-exposed to non-exposed surface is indicated by the *red arrow*. In addition, the vehicle in the bottom left (*red arrow*) moved out of the FOV after the lidar scanner collection but before the TIR collection. This is shown by the overlay of column temperature values on the truck 3-D point cloud.

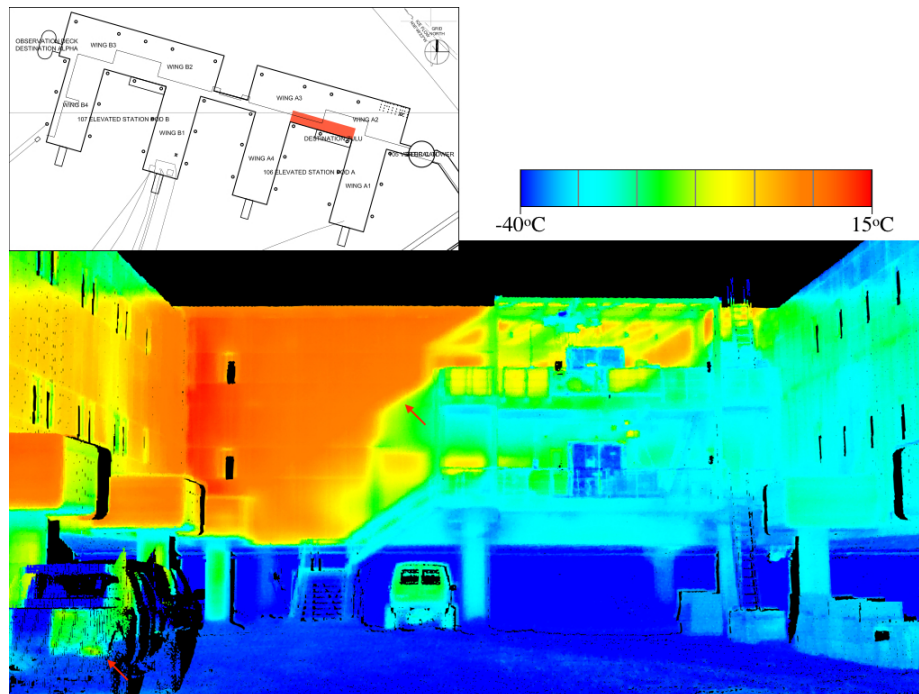


Figure 41. A 3-D thermal model of Wing A1 West. *Top left:* Focus section highlighted in *red* on the Elevated Station map. *Bottom:* Wing A1 West at a  $-40^{\circ}\text{C}$  to  $-10^{\circ}\text{C}$  scale. Thermal bridging is indicated by *red arrows* and is measured across the entire wall.

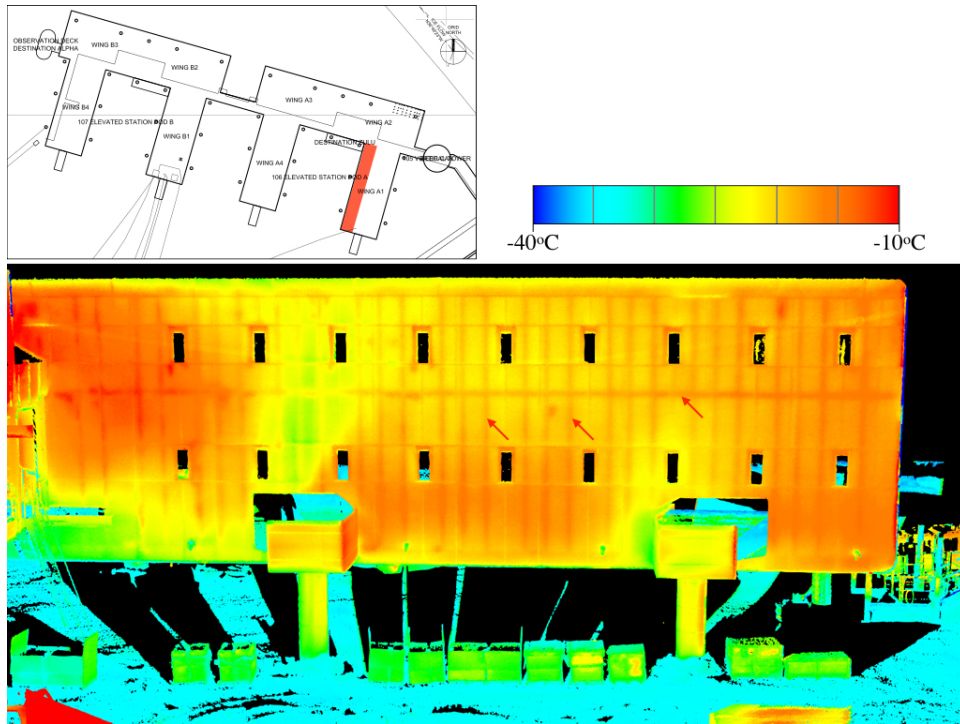


Figure 42. A 3-D thermal model of Wing A1 South. *Top left:* Focus section highlighted in *red* on the Elevated Station map. *Bottom:* Left and right views of Wing A1 South at a  $-15^{\circ}\text{C}$  to  $15^{\circ}\text{C}$  scale. Shadowing from direct solar exposure is visible in the bottom left image, below and left of the exterior stairwell.

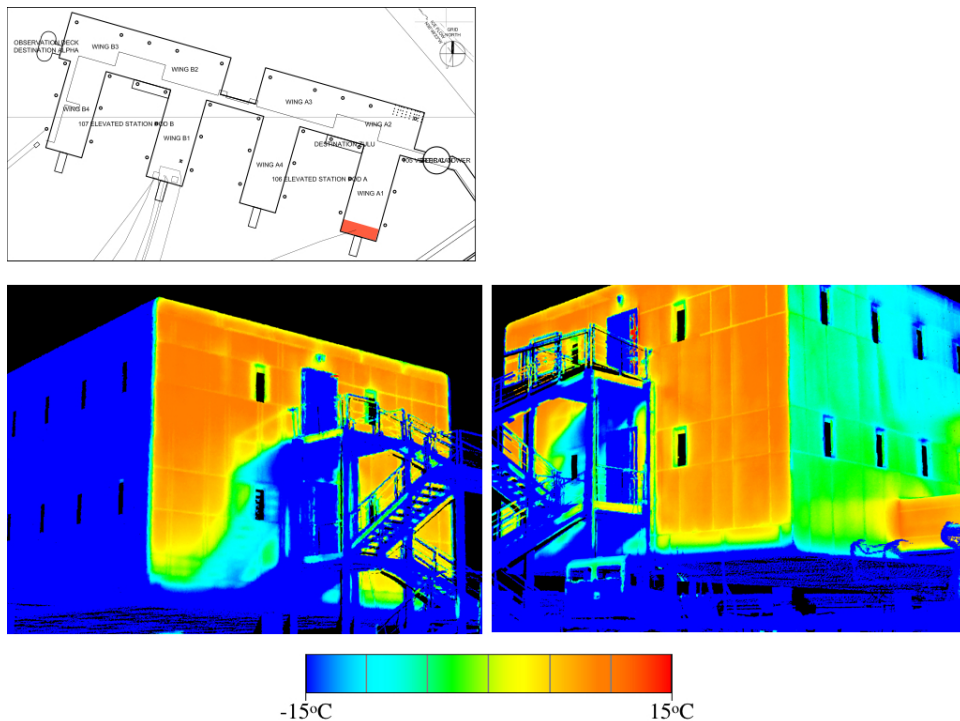


Figure 43. A 3-D thermal model of Wing A1 East. *Top left:* Focus section highlighted in red on the Elevated Station map. *Bottom:* Wing B1 East at a  $-40^{\circ}\text{C}$  to  $-10^{\circ}\text{C}$  scale.

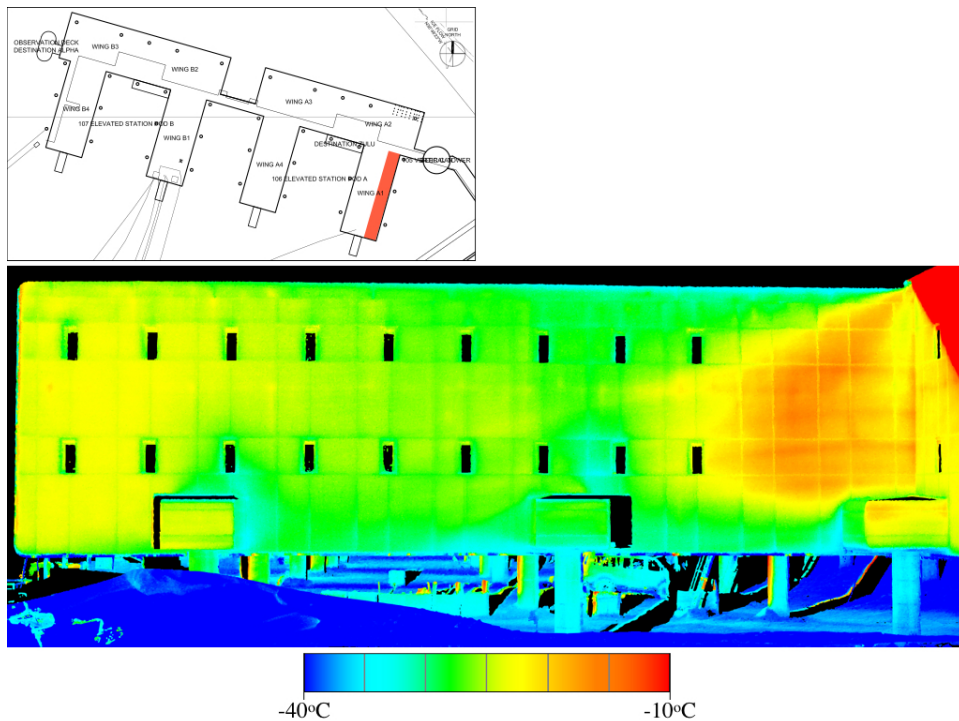


Figure 44. A 3-D thermal model of the Vertical Tower South. *Top left:* Focus section highlighted in red on the Elevated Station map. *Bottom:* Vertical Tower South at a  $-40^{\circ}\text{C}$  to  $20^{\circ}\text{C}$  scale. The transition line between solar-exposed and unexposed surfaces is indicated by red arrows. The Vertical Tower, made of corrugated metal, is highly reflective and therefore reflects the adjacent building surface temperatures.

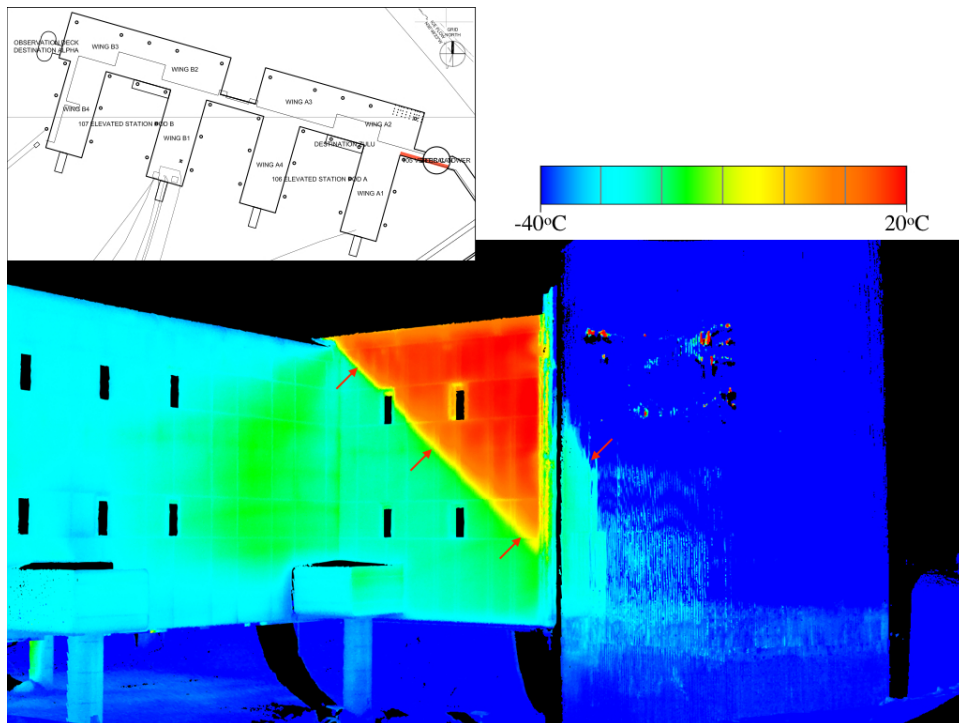
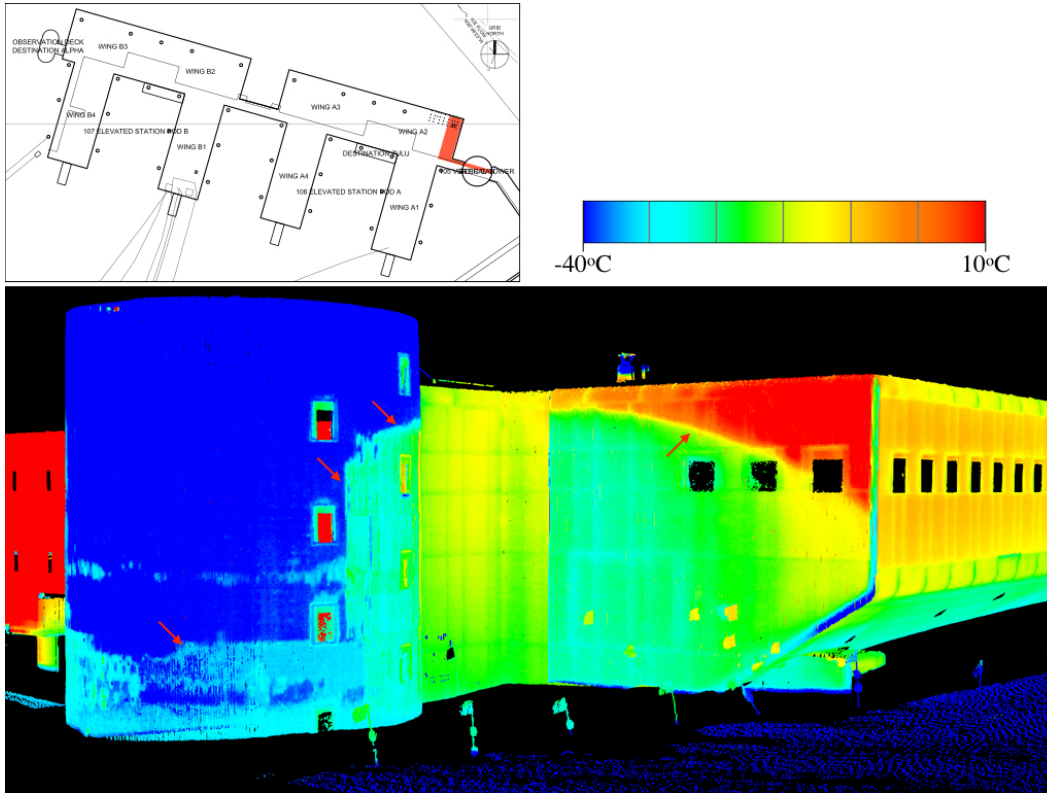


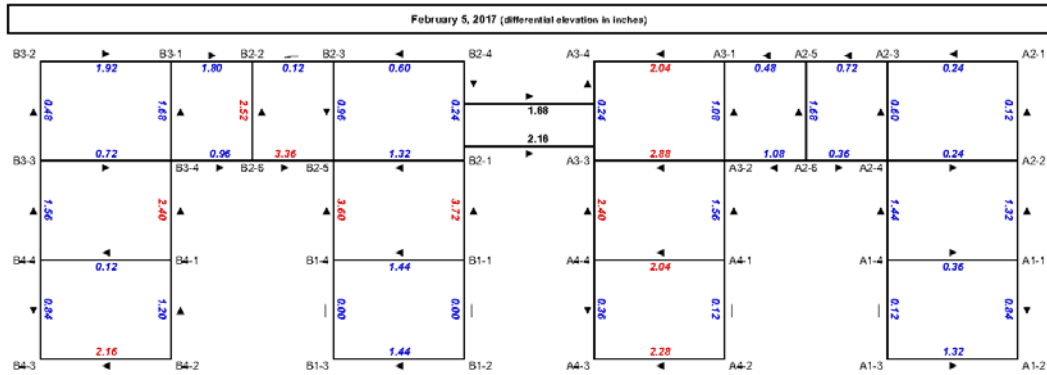
Figure 45. A 3-D thermal model of the Vertical Tower North and Wing A2 East. *Top left:* Focus section highlighted in *red* on the Elevated Station map. *Bottom:* Vertical Tower North and Wing A2 East at a  $-40^{\circ}\text{C}$  to  $10^{\circ}\text{C}$  scale. The transition line between solar exposed and unexposed surfaces is indicated by *red arrows*.



### 5.3 Elevated Station structural assessment

In addition to assigning temperature values in the 3-D model, the lidar-derived point cloud is useful for assessing the state of the building infrastructure. Knowing that the ice-sheet motion and snow accumulation and ablation would vary spatially and that there would be imbalanced weight distribution between the pods, the Elevated Station was design to be leveled periodically through the incremental extension of support columns. Each individual Pod (A and B) is connected to a buried platform via 18 support columns. Each column contains a  $90^{\circ}$  angle bar extending outside of the insulation panel, which is used in periodic height surveys to measure the amount of settlement at each column. From these measurements, a height change map is created to inform USAP for future leveling procedures. Figure 46 (and appendix Figure 1) shows the measured height differences between adjacent columns (blue and red values) from a 5 February 2017 survey, indicating changes greater than 2 in. in red. The arrows indicate the down-sloping direction (e.g., column B4-2 is 2.16 in. higher than B4-3).

Figure 46. Measured height differences between adjacent support columns of the South Pole Elevated Station from the 5 February 2017 traditional survey. The number values indicate the amount of height difference (*red* is greater than a 2 in. change, and *blue* is less than a 2 in. change) while the *arrows* indicate the down-sloping direction. See appendix Fig. 1 for large format.



Given that the 90° angle bars used for measuring column heights are easily identified within the lidar point cloud and that the point cloud is georeferenced and therefore height measurements can be made directly from the point cloud, it is possible to recreate the column height measurements from the point cloud (Figure 47). Because the traditional column survey was conducted less than 3 weeks after the lidar/TIR survey, the height differences measured by the lidar sensor will be similar to those measured by the traditional survey. Figure 48 (and appendix Figure 2) shows the height difference between adjacent columns as measured from the lidar point cloud. The values from the 17–18 January 2017 lidar survey can then be compared to the values from the 5 February 2017 traditional survey, as shown in Table 1.

With a standard deviation of 0.31 in. for all column height measurement comparisons, the lidar-derived settlement analysis appears to be a sufficient technique for validating the traditional survey methods or as a replacement process.

Figure 47. A point cloud side view of an isolated column from the Elevated Station, colored by surface reflectance. The angle bar extending from the column is indicated by the *red arrow*. Height measurements for the lidar-derived settlement analysis were made at the bottom end of the angle bar.

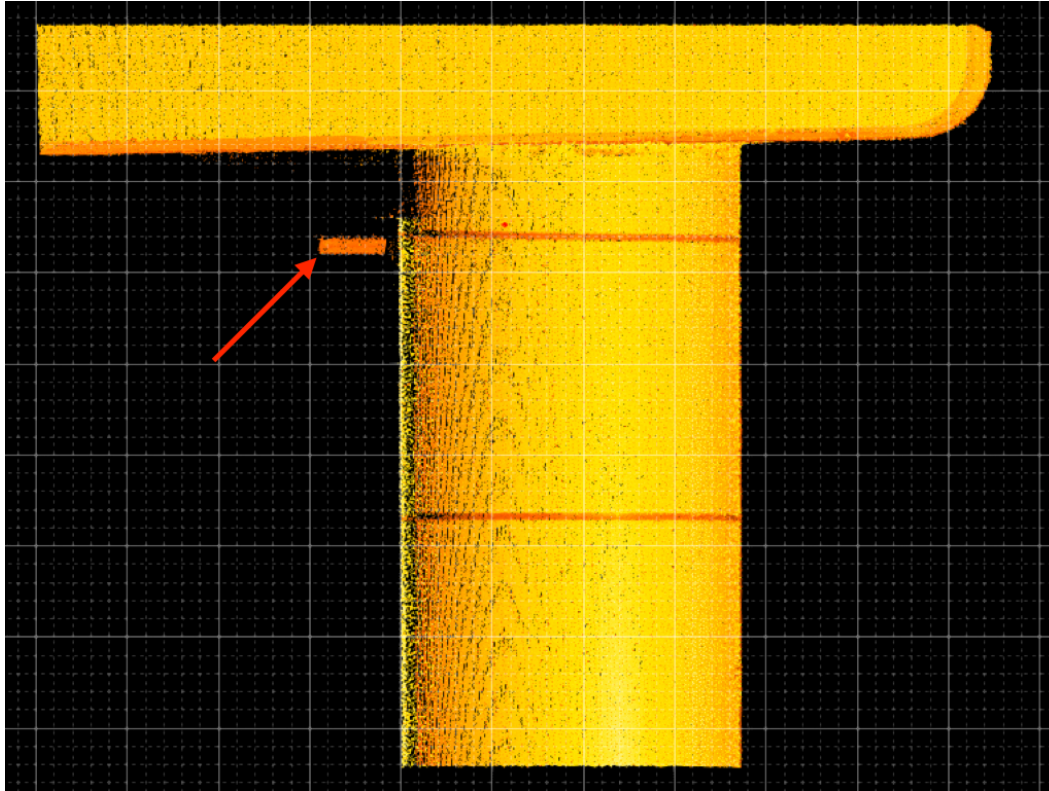


Figure 48. Measured height differences between adjacent support columns of the South Pole Elevated Station from the 17–18 January 2017 lidar survey. The number values indicate the amount of height difference (*red* is greater than a 2 in. change, and *blue* is less than a 2 in. change) while the *arrows* indicate the down-sloping direction. See appendix Fig. 2 for large format.

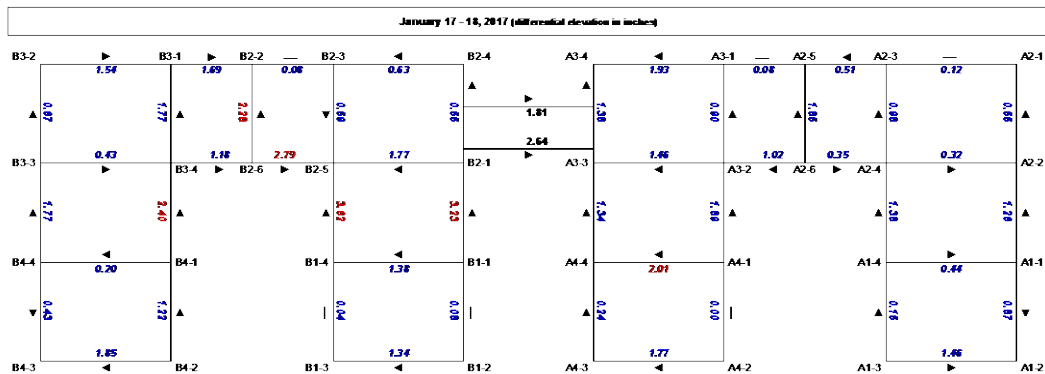


Table 1. Comparison between lidar-derived column angle bar measurements (17–18 January 2017) and traditional column survey measurements (5 February 2017). Values (inches) are the 5 February results subtracted from the 17–18 January results. The table is read by finding the top and bottom column associated with the measurement difference blocks, which have *white* backgrounds. For example, the measurement difference between columns A1-1 and A1-2 is 0.03 in. The standard deviation for all values is highlighted in *yellow*: 0.31 in.

Measurement Differences: 05Feb2017 subtracted from 17-18Jan2017							
Column	in Inches						
A1-1	0.03		0.08			1.32	
A1-2		0.14					
A1-3	0.03						
A1-4							
A2-1	0.43		0.08				-0.06
A2-2		-0.12					
A2-3	0.38			-0.21			
A2-4							
A2-5	0.17				-0.01		
A2-6						-0.40	
A3-1	-0.18		-0.11	-0.06			
A3-2		-1.42					
A3-3	1.14					0.33	
A3-4							
A4-1	-0.12		-0.03				-1.06
A4-2		-0.51					
A4-3	-0.12						
A4-4							
B1-1	0.08		-0.06				
B1-2		-0.10					
B1-3	0.04					-0.49	
B1-4							
B2-1							
B2-2	-0.04		0.45	0.31			0.02
B2-3		0.03					
B2-4					-0.24	-0.37	
B2-5	-0.57					-0.11	
B2-6							
B3-1	-0.38		0.09	0.22			
B3-2		0.19					
B3-3	-0.29						
B3-4							
B4-1	0.02		0.08			0.00	0.21
B4-2		-0.31					
B4-3	-0.41						
B4-4							

Pod A/B Link

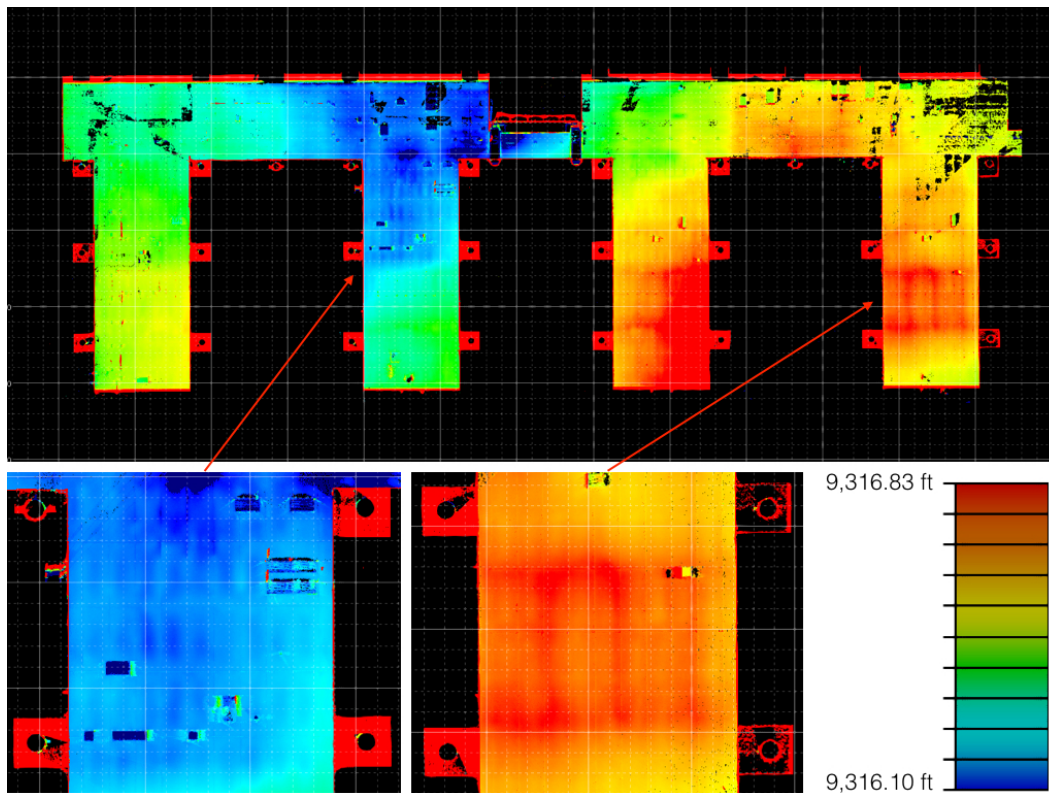
Standard Deviation 0.31

A3-4	0.13
B2-4	

A3-3	0.48
B2-1	

The benefit of the lidar survey is that the entire exterior surface of the Elevated Station (excluding the roof) is represented by a dense, high-accuracy point cloud. Therefore, in addition to quantifying point-to-point changes (column height measurements), it is possible to analyze vector and planar surfaces from the building exterior to provide a richer dataset for infrastructure assessments and settlement analysis. For example, by isolating the bottom surfaces of the Elevated Station and colorizing these points by height, trends in surface height changes become evident (Figure 49). While these results generally agree with the column measurements conducted on 5 February 2017, they also provide higher resolution information of localized deformation.

Figure 49. *Top:* Bottom surface of the Elevated Station isolated and colored by height (*blue to red* = 9,316.10 ft to 9,316.83 ft), clearly showing areas of settlement and building slope. The maximum height difference is approximately 8.7 in. Of note is the low point of Wing B1, which houses the emergency power generator, a large and heavy system compared to other sections of the station. *Bottom left:* Sagging of SIP is visible as gridded low points. *Bottom right:* Apparent frame structure is visible as orthogonal height points (*red grid*).



## 6 Conclusion and Recommendations

Between 17 and 19 January 2017, we collected a 3-D thermal model of the Amundsen-Scott South Pole Station's Elevated Station building by using a combined lidar/TIR scanning system in an effort to identify deficiencies in the building's thermal envelope and to collect information for future structural assessments. These data are intended to assist USAP in determining potential thermal-deficiency remediation steps, confirming effective design and construction techniques, and assisting in ongoing efforts in leveling the Elevated Station. Because of consistent temperatures below the minimum operational temperatures of the sensors, we developed a thermal jacket to provide active heating of the system during data collection at the South Pole. We collected supporting data to assist in processing and interpreting the lidar/TIR results, including exterior/interior air temperature measurements, Real-time Kinematic GNSS measurements of lidar reflectors, and handheld DSLR images.

We presented the results and preliminary 3-D thermal models to NSF during the data processing and analysis period of the project, summarizing our initial findings. Further data processing has produced a full 3-D thermal model representing the exterior surfaces of the Elevated Station at centimeter-scale point spacing. Every individual point measurement in these point clouds was assigned a temperature value based on coincident TIR imagery.

Overall, the Elevated Station's design and construction provides a tight thermal envelope with little significant heat loss observed by the lidar/TIR system. We did locate minor SIP trim-fit issues and variations in the performance of the station's windows and identified thermal bridging where heat was being transferred through the building's frame. Future design and construction techniques may avoid this by ensuring there is overlapping insulation between the exterior wall and internal frame. The entrance doorways displayed little to no heat loss, validating the use of the cold-room-style doors.

Through analysis of building column height differences, measurements of pod/wing slope, and comparison to data collected shortly after the lidar/TIR survey by the traditional building settlement survey techniques, we identified low and high points and areas of deformation between sections of the building. The lidar survey alone provides both validation for

current building settlement measurements and an alternative approach with the added value of a full 3-D model final product for further exploitation.

Given the homogeneity of the building's exterior through consistent use of the same windows and doors and the repeating patterns for the building's pods and wings, individual TIR images without the spatial reference provided by the lidar point cloud would be difficult to associate with specific locations on the building in follow up analysis. The combined lidar/TIR dataset avoids this difficulty through its 3-D data products.

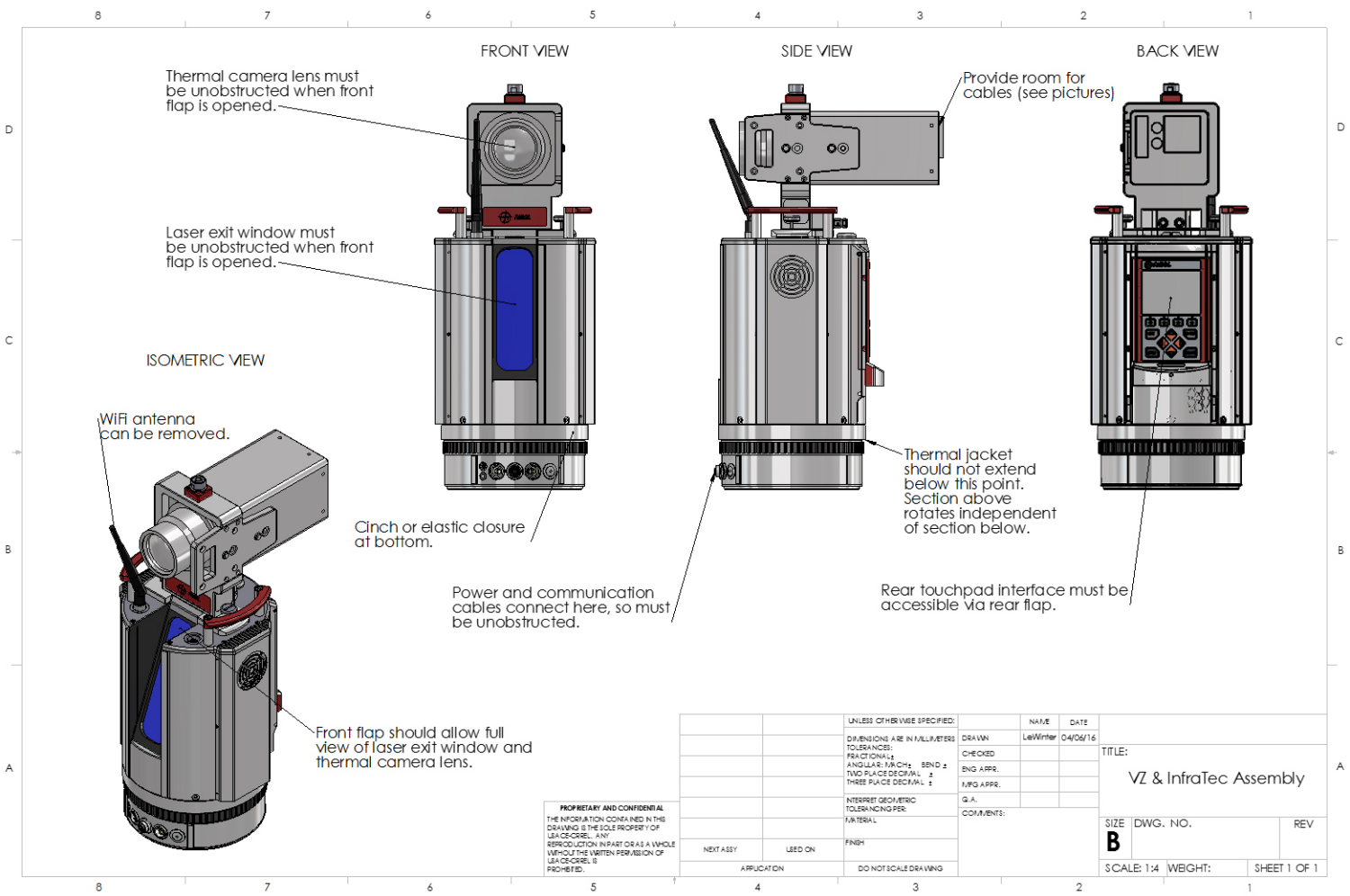
The final point clouds are available for NSF-personnel access and download through the Army Corps of Engineers Geospatial Repository and Data Management System (GRiD, <https://rsgis.erdcdren.mil/griduc/>) and through the ERDC online repository. Contact the authors for access instructions. Additionally, these data are indexed and loaded into a web-based 3-D viewer, allowing users to view the point clouds, query individual points, modify the temperature colorization scale, and make measurements without the need for specific software. Links to the web-based 2-D viewer are provided in GRiD. With these data available in GRiD, researchers will have readily available access to the full 3D thermal models for future exploitation.

## References

- Deeb, E. J., and A. LeWinter. 2018. *Building Envelope Assessment Using Thermal Infrared and Lidar Scanning: Palmer Station, Antarctica*. ERDC/CRREL TR-18-9. Hanover, NH: U.S. Army Engineer Research and Development Center.
- Lazzara, M., L. M. Keller, T. Markle, and J. Gallagher. 2012. Fifty-Year Amundsen–Scott South Pole Station Surface Climatology. *Atmospheric Research* 118 (15 November 2012): 240–259. <http://dx.doi.org/10.1016/j.atmosres.2012.06.027>.
- Phetteplace, G. 2007. *Infrared Survey of the Elevated Station 2006–2007 Season, South Pole, Antarctica*. ERDC/CRREL LR-07-09. Hanover, NH: U.S. Army Engineer Research and Development Center.
- Vasel, B. 2018. Meteorological Measurements from the NOAA/ESRL/GMD Baseline Observatories, South Pole, Antarctica (SPO). [www.erl.noaa.gov/gmd/obop/spo/](http://www.erl.noaa.gov/gmd/obop/spo/) (accessed January 2018).

---

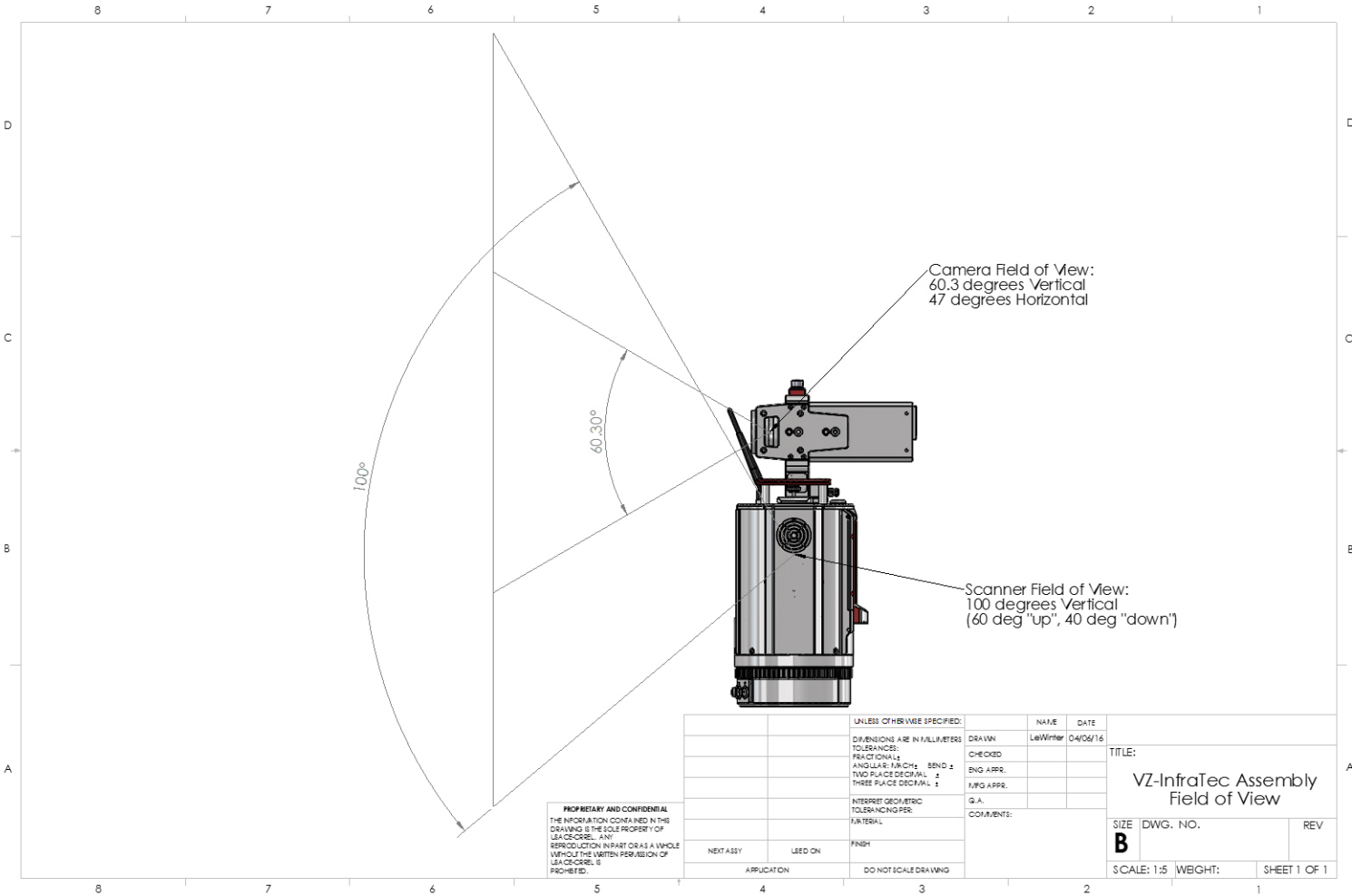
## **Appendix A: Lidar/TIR System Thermal Jacket Design**



**PROPRIETARY AND CONFIDENTIAL**  
 THE INFORMATION CONTAINED IN THIS DRAWING IS THE SOLE PROPERTY OF LEACORE, INC. ANY REPRODUCTION IN WHOLE OR AS A WHOLE WITHOUT THE WRITTEN PERMISSION OF LEACORE, INC. IS PROHIBITED.

		UNLESS OTHERWISE SPECIFIED:	NAME	DATE
		DIMENSIONS ARE IN MILLIMETERS	DRAWN	LeWinter 04/06/16
		TOLERANCES:	CHECKED	
		FRACTIONAL:	ENG APPR.	
		ANGULAR: $\pm 0.05^\circ$ BEND $\pm 0.1^\circ$	MFG APPR.	
		TWO PLACE DECIMAL: $\pm 0.05$		
		THREE PLACE DECIMAL: $\pm 0.025$		
		INTERPRET GEOMETRIC TOLERANCING PER: ASME Y14.5-2009		
		MATERIAL:		
		FINISH:		
		APPLICATION		
		DO NOT SCALE DRAWING		

TITLE:	
VZ & InfraTec Assembly	
SIZE	DWG. NO.
<b>B</b>	
SCALE: 1:4	WEIGHT:
	SHEET 1 OF 1

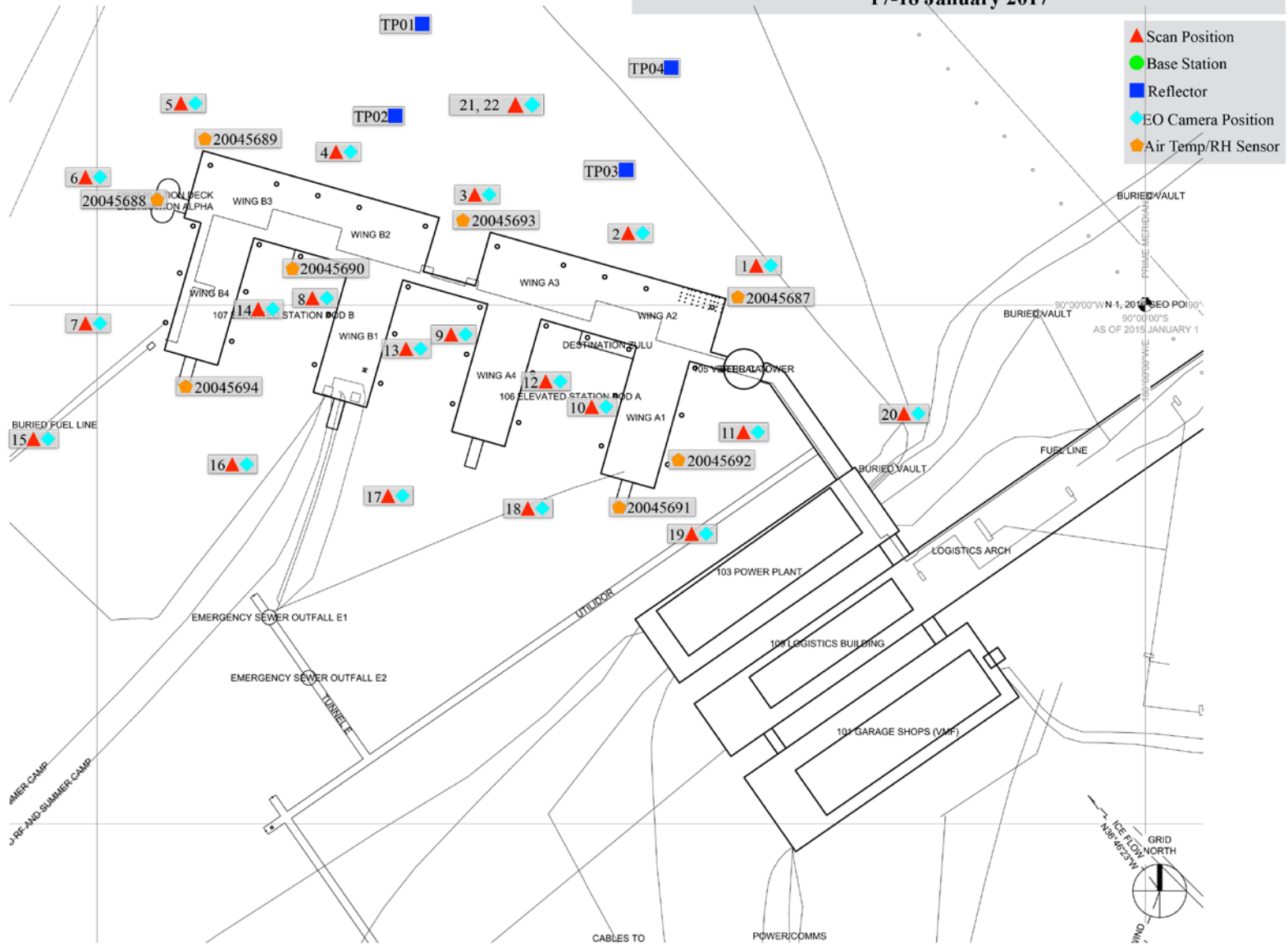


**PROPRIETARY AND CONFIDENTIAL**  
THE INFORMATION CONTAINED IN THIS DRAWING IS THE SOLE PROPERTY OF USA/CS/CRREL. ANY REPRODUCTION IN PART OR AS A WHOLE WITHOUT THE WRITTEN PERMISSION OF USA/CS/CRREL IS PROHIBITED.

UNLESS OTHERWISE SPECIFIED:		NAME	DATE	TITLE:	
DIMENSIONS ARE IN MILLIMETERS		DRAWN	LeeWright	VZ-InfraTec Assembly	
TOLERANCES:		CHECKED		Field of View	
FRACTIONAL		ENG APPR.		SIZE	DWG. NO.
ANGULAR: 1/4 CHG; 3/32 2		ENG APPR.		<b>B</b>	REV
TWO PLACE DECIMAL 1		ENG APPR.		SCALE: 1:5	WEIGHT:
THREE PLACE DECIMAL 1		COMMENTS:		SHEET 1 OF 1	
INTERPRET GEOMETRIC TOLERANCING PER: MATERIAL					
NEXT ASSY	USED ON	FINISH			
APPLICATION	DO NOT SCALE DRAWING				

## **Appendix B: 2017 Lidar/TIR Survey Map**

# Amundsen-Scott South Pole Station LiDAR/Thermal Infrared Survey 17-18 January 2017



# Appendix C: CRREL Lidar/TIR System Data Acquisition Procedure

January 2017 South Pole Station

## C.1 Overview

This document describes the acquisition procedure for capturing coregistered thermal images using the InfraTec VarioCAM HD camera and Riegl VZ-1000 terrestrial laser scanner.

## C.2 Acquisition PC Setup

### C.2.1 Network

1. Set LAN networks connection to the following settings:
  - a. IP address: 192.168.2.2
  - b. Subnet mask: 255.255.255.0
2. Ensure RiSCAN Pro (RSP) and IRBIS 3 Professional is installed
3. When scanner is powered, select the Wi-Fi S9998518, password 123456789.
4. Connect InfraTec Ethernet cable to laptop, and check connection via cmd if necessary.

### C.2.2 RiSCAN Pro Setup

1. Create a new project.
2. In the project attributes, set the following:
  - a. Instrument Tab, Scanner IP: 10.0.0.1 (if using wireless) 192.168.2.125 (if using network cable. Note that this was changed to work with the InfraTec address.)
  - b. Camera model: Custom camera
3. Set image acquisition to external software:
  - a. Tools>Options>Image acquisition
  - b. Image acquisition controlled by: Software
4. Set Camera and Mounting calibrations
  - a. Camera: Result calibration nikonD700\_2505549\_20mm\_Final\_4256x2832

- b. Mounting: Result mounting nikonD700\_2505549\_20mm\_Final

### **C.2.3 InfraTec IRBIS 3 Professional Setup**

1. Camera IP address is preset to 192.168.2.15
2. Open IRBIS 3 Professional.
3. Ensure that the scanner is powered and the camera is initialized.
4. In Camera tab, select “Connect.”
5. Use VarioCAM HD; the camera will connect and display a live image.
6. Select the “Remote” tab to display the focus options.
7. Go to the “View” tab.
8. Select the “Scale” tab.
9. Return to the “Camera” tab.
10. Use the “Live” tab to see a live view.
11. In the “Snap” tab, ensure it is set to “Premium and Auto save.”

## **C.3 Hardware Setup**

1. Attach the scanner to the survey tripod.
2. Attach the InfraTec VarioCAM HD TIR camera to the scanner.
3. Assemble the thermal jacket and install it on the lidar/TIR system.
  - a. Ensure that the jacket does not impede system rotation when installed.
  - b. Feed the TIR Ethernet cable through the thermal jacket rear panel.

## **C.4 Collection of Data**

1. In RiSCAN Pro collect a scan with settings appropriate to the project, but do not acquire the images automatically.
2. After the scan is complete, right-click the scan and select “Image acquisition.” (If using the network cable with the scanner, switch project to wireless [10.0.0.1], disconnect scanner network cable, and connect the InfraTec network cable.)
3. Use the “NikonD700\_2505549\_20mm\_Final Scanner” camera calibration/mounting file.
4. Use a 40% overlap to ensure good coverage of the scan area.
5. The scanner will move to the first image phi angle and prompt the user to capture the image.
6. Go into IRBIS 3 and focus the camera; then select “Snap,” and verify that the new image with naming convention YYMMDD\_HHMMSS.irb was saved.

7. Back in RSP, select “OK” to proceed with the next image.
8. Proceed for all images.
9. End the scan position, and proceed to the next position.

## **Appendix D: 2017 Lidar/TIR Survey Notes**

Amundsen-Scott South Pole Station LiDAR/TIR Survey Notes

Date (local)	Scan Position	Focus Area	Scan Start Time (GMT)	Image Start Time (GMT)	SPO Station AirTemp (C)	Notes
2017/1/17	001	Wing A2	2017-01-17 0:54:10	2017-01-17 1:06:00	-28.2	Clear with low wind, small amount of blowing snow
	002	Wing A2, A3	2017-01-17 1:39:43	2017-01-17 1:54:00	-27.8	Clear with low wind, small amount of blowing snow
	003	Wing A3, B2, Bridge	2017-01-17 2:05:37	2017-01-17 3:15:00	-28.9	Clear with low wind, small amount of blowing snow
	004	Wing B2, B3	2017-01-17 3:20:08	2017-01-17 3:31:00	-29.3	Sunny, though sun not on survey area of interest
	005	Wing B3	2017-01-17 3:35:06	2017-01-17 3:44:00	-29.5	Sunny, though sun not on survey area of interest
	006	Observation Deck	2017-01-17 3:46:49	2017-01-17 3:56:00	-30.0	Sunny, though sun not on survey area of interest
	007	Wing B4	2017-01-17 4:15:17	2017-01-17 4:23:00	-29.8	Sunny, end of survey for the day due to direct sun on next area of interest
2017/1/18	008	Wing B4, Inner	2017-01-17 20:14:51	2017-01-17 20:28:00	-27.6	Scan between B1 and B4, do not use B1 thermal images due to direct sun
	009	Wing B1, Inner	2017-01-17 20:31:09	2017-01-17 20:43:00	-27.7	Scan between B1 and A4, do not use A4 thermal images due to direct sun
	010	Wing A4, Inner	2017-01-17 20:49:47	2017-01-17 21:05:00	-26.7	Scan between A4 and A1, do not use A1 thermal images due to direct sun
	011	Wing A1, Outer	2017-01-17 21:12:54	2017-01-17 21:25:00	-26.9	Sunny, but not directly on A1 outer, OK to use thermal
	012	Wing A1, Inner	2017-01-18 0:05:02	2017-01-18 0:17:00	-26.9	Scan between A4 and A1, do not use A4 thermal images due to direct sun
	013	Wing A4, Inner	2017-01-18 0:20:05	2017-01-18 0:33:00	-27.3	Scan between B1 and A4, do not use B1 thermal images due to direct sun
	014	Wing B1, Inner	2017-01-18 0:44:45	2017-01-18 0:56:00	-27.5	Scan between B1 and B4, do not use B4 thermal images due to direct sun
	015	Wing B4, Outer, End	2017-01-18 1:03:02	2017-01-18 1:14:00	-27.8	Scattered clouds, sun intermittently on end of wings, use different thermal scale
	016	Wing B1, B4, Ends	2017-01-18 1:16:28	2017-01-18 1:25:00	-27.9	Scattered clouds, sun intermittently on end of wings, use different thermal scale
	017	Wing B1, A4, Ends	2017-01-18 1:28:25	2017-01-18 1:38:00	-28.1	Scattered clouds, sun intermittently on end of wings, use different thermal scale
	018	Wing A4, A1, Ends	2017-01-18 1:38:45	2017-01-18 1:48:00	-27.6	Scattered clouds, sun intermittently on end of wings, use different thermal scale
	019	Wing A1, Inner, End	2017-01-18 1:50:21	2017-01-18 2:01:00	-26.9	Scattered clouds, sun intermittently on end of wings, use different thermal scale
	020	Wing A1, A2	2017-01-18 2:05:00	2017-01-18 2:15:00	-27.2	Scattered clouds
	021	Wing A2, A3, B2, B3	2017-01-18 2:22:37	2017-01-18 2:36:00	-27.2	Scattered clouds, no sun on area of interest, can use inclination for 1st scan
2017/1/19	022	Wing A2, A3, B2, B3	2017-01-18 22:31:26	2017-01-18 22:47:00	-24.3	Registration scan position & reflector survey: Use inclination from 1st scan

## **Appendix E: South Pole Elevated Station Lidar/TIR Survey: Lidar Processing Notes**

### **E.1 Overview**

This documents the steps and processes conducted on data collected by Adam LeWinter and David Finnegan (CRREL) at the South Pole Station in January 2017. The team used a Riegl VZ-1000 with an InfraTec VarioCAM HD thermal infrared camera. The system was deployed in a custom thermal heating jacket.

### **E.2 Thermal Image Rename**

1. For each scan position, the thermal images collected externally with the InfraTec camera have the naming convention YYMMDD\_HHMMSS.irb.
2. Use the Bulk Rename Utility and the InfraTec\_irb\_rename.bru setting file to rename the .irb files in the RiSCAN Pro naming convention (ScanPosXXX – Image00X).

### **E.3 Export thermal images as JPG files for static point cloud colorization**

This process assigns an RGB value to the point cloud based on a static temperature scale palette set in IRBIS 3.

1. Open .irb files in IRBIS 3.
2. Select the temperature range appropriate for the imagery and temperatures measured.
  - a. Temperature range:  $-5$  to  $-45^{\circ}\text{C}$
  - b. Palette: VarioCAM
3. Deselect “Scale” tab so only the image is displayed.
4. Export the JPG file into the “RiSCAN Pro folder”  
/SCAN/ScanPosXXX/SCANPOSIMAGES.

### **E.4 Colorize scan position data in Riegl RiSCAN Pro Software**

1. Delete all Nikon camera and mounting calibrations.
2. Import Infratec\_VarioCAM\_HD\_15mm\_11-16-2015\_Preston.cam and .dat files into the camera and mounting calibrations.

3. Assign calibrations to all scan positions.
4. Run “Color from Images” for each scan, and verify that the colorization is correct.

## **E.5 Georeference data to global coordinate system**

1. Use data collected during the reflector survey onsite during the last day of scanning for ScanPos022.
2. Set the Coordinate Reference System:
  - a. UPS South Projection
  - b. WGS84 Datum
  - c. EGM96(Global) geoid
3. Create 201701\_SouthPole\_Reflector\_Survey project in Trimble Business Center.
4. Run baseline processing in Trimble Business Center.
5. Export all points in UPS South Projection, Northing, Easting, Elevation.
6. In .csv file, create average values for each reflector observation and average the 2 observations (e.g. TP1-average).
7. Adjust elevation to account for quick release (0.0812 m) and cylinder height (0.05 m), name Elevation (adjusted).
8. Import .csv values into RiSCAN Pro GLCS and remove all but the TP(x)-average and base station (5012LIDAR) points.
9. Calculate POP matrix, freeze POP matrix.
10. Copy GLCS to PROCS.
11. Using ScanPos022, run “Find corresponding points” to tie reflectors to GLCS.
12. Freeze the ScanPos022 SOP matrix.

## **E.6 Register scan positions**

1. Since ScanPos009 is tilted between the two scans, export the second scan as a .laz file, then import as a Point cloud object into ScanPos009b.
2. Run Extract Plane Patches for Multi-Station Adjustment processing.
  - a. Settings: default
    - (1) Minimum point count: 50
    - (2) Max Std. Dev: 0.020 m
    - (3) Max Deviation: 20
    - (4) Min. Reflectance: -15 db
3. Run coarse adjustment/MSA in the following order:

- 
- a. ScanPos021, 003, 002, 004, 005, 001, 006, 007, 015, 016, 017, 018, 019, 011, 020, 014, 008 (NOTE THAT BOWING/BUBBLING IS OBSERVED ON SIPS PANELS ABOVE SCANPOS008 POSITION), 013, 009, 009b, 012, 010

# Appendix F: 2017-01-SouthPole Processing Report

## F.1 Spatial Reference System

All data are provided in UPS South, WGS84, using the EGM96(Global) geoid. When appropriate, EPSG:32761+5773 was used.

## F.2 Attributing point clouds with thermal imagery

Twenty-two scan positions in total were attributed, one scan per scan position. Scan positions were named ScanPos001 through ScanPos022, and ScanPos009 was split into ScanPos009 and ScanPos009b. Images 010 through 012 were moved from ScanPos009 to ScanPos009b, and the scan 170117\_204129.rxp was moved from ScanPos009 to ScanPos009b.

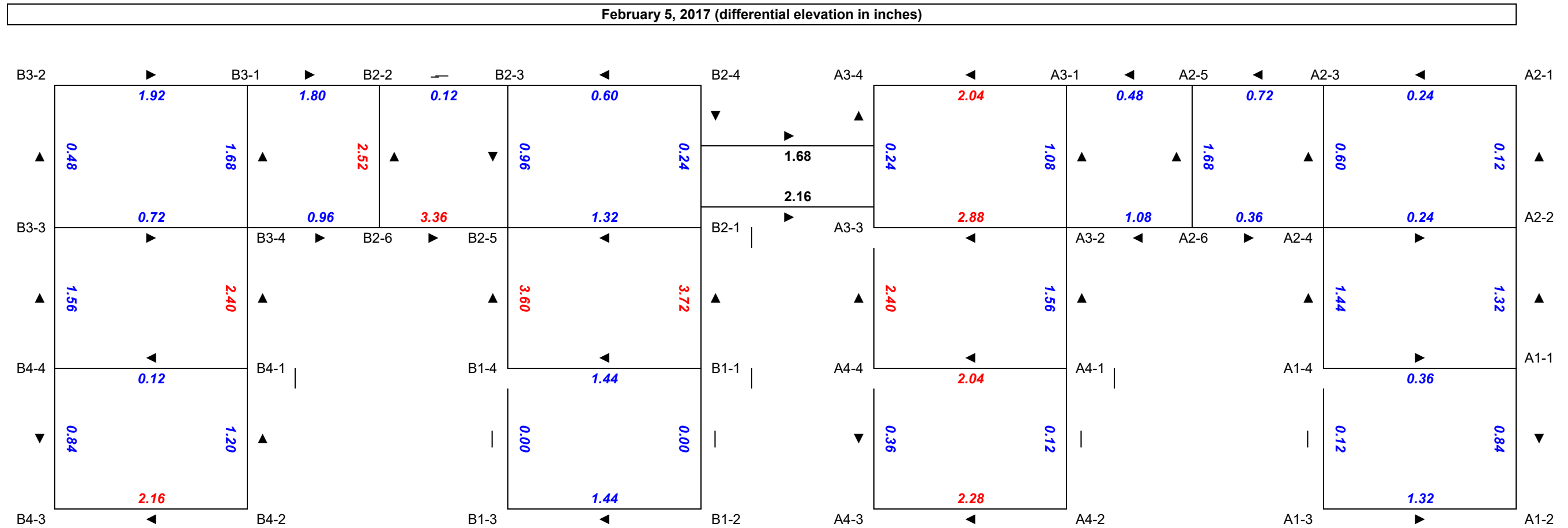
Point cloud attribution with thermal imagery followed this algorithm:

1. Each thermal image has an .irb extension and a file name in the following format: ScanPosXXX – ImageXXX.irb. For each thermal image, the scan position and image name are extracted.
2. The RiSCAN Pro project file (project.rsp) is used to extract the calibration parameters for each scan position and image. Extraction is done with the RiSCAN Pro Software Library.
3. For each scan position, open the scan position's .rxp file (using Riegl's scanifc library via an external software interface) and read each point.
4. For each point, search the active scan position's images for coincident imagery. The math used to convert Scanner's Own Coordinate System points into image pixels is taken from Riegl's own software documentation.
5. All overlapping pixels are averaged to produce an average temperature for that point.
6. The "gps\_time" field of the point is set to the average temperature in degrees Celsius. A continuous color scale, from blue to red, is used to set the color of the point from the average temperature.
7. The point is written out to a LAS file.
8. One LAS file is written for each scan position.

Once each scan position has a colorized, attributed output LAS file, each file is resampled to 0.02 m via a Poisson sampling, filtered to remove outlier points, and converted to a compressed laz file. All source files are also combined into a single master file using the same procedure.

# Appendix G: Elevated Station Column Height Elevation Plots

Figure G-1. February 5, 2017 Elevated Station column height difference map





# REPORT DOCUMENTATION PAGE

*Form Approved*  
*OMB No. 0704-0188*

Public reporting burden for this collection of information is estimated to average 1 hour per response, including the time for reviewing instructions, searching existing data sources, gathering and maintaining the data needed, and completing and reviewing this collection of information. Send comments regarding this burden estimate or any other aspect of this collection of information, including suggestions for reducing this burden to Department of Defense, Washington Headquarters Services, Directorate for Information Operations and Reports (0704-0188), 1215 Jefferson Davis Highway, Suite 1204, Arlington, VA 22202-4302. Respondents should be aware that notwithstanding any other provision of law, no person shall be subject to any penalty for failing to comply with a collection of information if it does not display a currently valid OMB control number. **PLEASE DO NOT RETURN YOUR FORM TO THE ABOVE ADDRESS.**

<b>1. REPORT DATE (DD-MM-YYYY)</b> June 2018			<b>2. REPORT TYPE</b> Technical Report/Final			<b>3. DATES COVERED (From - To)</b>		
<b>4. TITLE AND SUBTITLE</b> Building Envelope and Infrastructure Assessment Using an Integrated Thermal Imaging and Lidar Scanning System: Amundsen-Scott South Pole Station, Antarctica						<b>5a. CONTRACT NUMBER</b>		
						<b>5b. GRANT NUMBER</b>		
						<b>5c. PROGRAM ELEMENT NUMBER</b>		
<b>6. AUTHOR(S)</b> Adam L. LeWinter, David C. Finnegan, Elias J. Deeb, and Peter J. Gadomski						<b>5d. PROJECT NUMBER</b>		
						<b>5e. TASK NUMBER</b> EP-ANT-16-07		
						<b>5f. WORK UNIT NUMBER</b>		
<b>7. PERFORMING ORGANIZATION NAME(S) AND ADDRESS(ES)</b> U.S. Army Engineer Research and Development Center (ERDC) Cold Regions Research and Engineering Laboratory (CRREL) 72 Lyme Road Hanover, NH 03755-1290						<b>8. PERFORMING ORGANIZATION REPORT NUMBER</b>  ERDC/CRREL TR-18-10		
<b>9. SPONSORING / MONITORING AGENCY NAME(S) AND ADDRESS(ES)</b> National Science Foundation, Office of Polar Programs 2415 Eisenhower Avenue Alexandria, VA 22314						<b>10. SPONSOR/MONITOR'S ACRONYM(S)</b> NSF		
						<b>11. SPONSOR/MONITOR'S REPORT NUMBER(S)</b>		
<b>12. DISTRIBUTION / AVAILABILITY STATEMENT</b> Approved for public release; distribution is unlimited.								
<b>13. SUPPLEMENTARY NOTES</b> Engineering for Polar Operations, Logistics, and Research (EPOLAR)								
<b>14. ABSTRACT</b> <p>We conducted a combined lidar and Thermal Infrared (TIR) survey at the Amundsen-Scott South Pole Station, Antarctica, in January 2017 to assess the building thermal envelope and infrastructure of the Elevated Station. These coregistered data produce a three-dimensional (3-D) model with assigned temperature values for target surfaces, useful in spatially identifying thermal anomalies and areas for potential improvements. In addition, the accuracy of the resulting 3-D point cloud is useful for assessing building infrastructure by locating and quantifying areas of building settlement and structural anomalies. The lidar/TIR data collection was conducted in tandem with interior and exterior temperature and atmospheric measurement logging, handheld electro-optical imagery collection, and Global Navigation Satellite System real-time kinematic surveys to place the collected data in a global coordinate system. By analyzing the resulting data products, we conclude that while some thermal deficiencies exist, the building design and the material have maintained thermal-envelope integrity and display no significant thermal deficiencies. However, comparing building base elevations shows that significant and unequal settlement across the building has occurred. We suggest mitigating the thermal deficiencies through exterior repairs and that the building settlement be addressed in future leveling procedures to include lidar surveys.</p>								
<b>15. SUBJECT TERMS</b> Antarctica, Buildings--Cold regions, Buildings--Heating and ventilation, Buildings--Insulation, Buildings--Thermal properties, EPOLAR, NSF, Optical radar, Thermography								
<b>16. SECURITY CLASSIFICATION OF:</b>				<b>17. LIMITATION OF ABSTRACT</b>	<b>18. NUMBER OF PAGES</b>	<b>19a. NAME OF RESPONSIBLE PERSON</b>		
<b>a. REPORT</b> Unclassified	<b>b. ABSTRACT</b> Unclassified	<b>c. THIS PAGE</b> Unclassified		SAR	75	<b>19b. TELEPHONE NUMBER (include area code)</b>		